Insights into the Mechanism of Deubiquitination by JAMM Deubiquitinases from Cocrystal Structures of the Enzyme with the Substrate and Product

Rashmi K. Shrestha,[†] Judith A. Ronau,[†] Christopher W. Davies,[†] Robert G. Guenette,[‡] Eric R. Strieter,[‡] Lake N. Paul,[§] and Chittaranjan Das*,[†]

[†]Department of Chemistry, Purdue University, 560 Oval Drive, West Lafayette, Indiana 47907, United States
[‡]Department of Chemistry, University of Wisconsin—Madison, 1101 University Avenue, Madison, Wisconsin 53706, United States
[§]Bindley Biosciences Center, Purdue University, West Lafayette, Indiana 47907, United States

ⓢ *Supporting Information*

ABSTRACT: AMSH, a conserved zinc metallo deubiquitinase, controls downregulation and degradation of cell-surface receptors mediated by the endosomal sorting complexes required for transport (ESCRT) machinery. It displays high specificity toward the Lys63-linked polyubiquitin chain, which is used as a signal for ESCRT-mediated endosomal—lysosomal sorting of receptors. Herein, we report the crystal structures of the catalytic domain of AMSH orthologue Sst2 from fission yeast, its ubiquitin (product)-bound form, and its Lys63-linked diubiquitin (substrate)-bound form at 1.45, 1.7, and 2.3 Å, respectively. The structures reveal that the P-side product fragment maintains nearly all the contacts with the enzyme as seen with the P portion (distal ubiquitin) of the Lys63-linked diubiquitin substrate, with additional coordination of the Gly76 carboxylate group of the product with the active-site Zn^{2+}. One of the product-bound structures described herein is the result of an attempt to cocrystallize the diubiquitin substrate bound to an active site mutant presumed to render the enzyme inactive, instead yielding a cocrystal structure of the enzyme bound to the P-side ubiquitin fragment of the substrate (distal ubiquitin). This fragment was generated *in situ* from the residual activity of the mutant enzyme. In this structure, the catalytic water is seen placed between the active-site Zn^{2+} and the carboxylate group of Gly76 of ubiquitin, providing what appears to be a snapshot of the active site when the product is about to depart. Comparison of this structure with that of the substrate-bound form suggests the importance of dynamics of a flexible flap near the active site in catalysis. The crystal structure of the Thr319Ile mutant of the catalytic domain of Sst2 provides insight into structural basis of microcephaly capillary malformation syndrome. Isothermal titration calorimetry yields a dissociation constant (K_D) of 10.2 ± 0.6 μM for the binding of ubiquitin to the enzyme, a value comparable to the K_M of the enzyme catalyzing hydrolysis of the Lys63-linked diubiquitin substrate (~20 μM). These results, together with the previously reported observation that the intracellular concentration of free ubiquitin (~20 μM) exceeds that of Lys63-linked polyubiquitin chains, imply that the free, cytosolic form of the enzyme remains inhibited by being tightly bound to free ubiquitin. We propose that when AMSH associates with endosomes, inhibition would be relieved because of ubiquitin binding domains present on its endosomal binding partners that would shift the balance toward better recognition of polyubiquitin chains via the avidity effect.
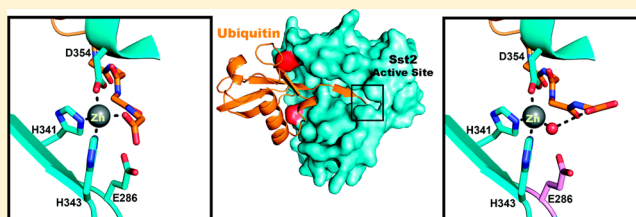
U biquitination, covalent attachment of the 76-amino acid protein ubiquitin to target proteins, controls a wide array of cellular functions, including protein quality control, cell cycle progression, transcription, endocytosis, DNA repair, and cellular signaling.[1−5] Ubiquitin is attached to target proteins via an isopeptide bond linking the side-chain amino group of lysine residues of the target to the terminal carboxylate group of ubiquitin (Gly76). This modification is allowed by the sequential catalytic activity of three enzymatic systems: E1 (ubiquitin-activating enzyme), E2 (ubiquitin-conjugating enzyme), and E3 (ubiquitin ligase).[6,7] The more widely understood form of ubiquitination involves the attachment of a polyubiquitin chain in which successive ubiquitin groups are linked to one of the seven lysines, or the N-terminal amino

group of the preceding monomer, to generate homopolymeric structures of one of eight linkage types. Polyubiquitin chains of distinct three-dimensional architecture are thus generated depending on which amino group of ubiquitin is used for chain extension (lysine 6, 11, 27, 29, 33, 48, or 63 or the amino group of Met1). A polyubiquitin chain of a given linkage type signifies a specific type of functional outcome.[5,8−10] For example, Lys48 (K48)-linked chains and, to some extent, K11-linked chains usually serve as the signal for proteasomal degradation, whereas K63 chains signal other types of

functions, such as DNA repair, endosomal–lysosomal sorting, and NF-κB signaling.[5,11]

Ubiquitination is a reversible post-translational modification like phosphorylation. Deubiquitinating enzymes, or DUBs, can hydrolytically remove ubiquitin from protein adducts to counteract ubiquitination. Accordingly, DUBs are known to play key regulatory roles in numerous cellular processes that rely on ubiquitination.[12,13] The human genome encodes approximately 100 DUBs, and most of their biological functions are yet to be determined. They can be grouped into five major families based on the structure of their catalytic domain: ubiquitin specific proteases (USPs), ubiquitin C-terminal hydrolases (UCHs), ovarian tumor proteases (OTUs), JAB1/MPN/MOV34 metalloenzymes (JAMMs), and Machado-Josephin domain proteases (MJDs).[14,15] Mechanistically, these enzymes can be divided into two main groups: cysteine proteases and zinc metalloproteases. The zinc metalloproteases consist of only one family, the JAMMs, whereas the other four families are cysteine proteases.[14,16,17]

The JAMM family of metallo DUBs is mechanistically related to the well-known metalloprotease thermolysin, despite having sequences substantially different from that of thermolysin. Generally, the active sites of thermolysin-like metalloproteases contain a Zn^{2+} ion coordinated by two histidines, an aspartate (or a glutamate), and a water molecule. The water molecule is held in place by hydrogen bonding with a different glutamate residue from the second coordination sphere, in addition to the metal ion, and acts as the nucleophile during the hydrolysis reaction.[16,18−20] Of the 14 JAMM proteins in the human genome, only seven contain a complete set of conserved residues needed for Zn^{2+} coordination in the active site, six of which, AMSH, AMSH-LP (AMSH-like protein), BRCC36, RPN11 (POH1), MYSM1, and CSN5, are known to have isopeptidase activity toward proteins conjugated to ubiquitin or ubiquitin-like modifiers.[14,16,17,20−27]

Endocytic sorting of cell-surface receptors to lysosomes for their degradation is executed by the ESCRT (endosomal sorting complexes required for transport) machinery, which consists of four different macromolecular assemblies, ESCRT-0, -I, -II, and -III.[28,29] Internalized receptors (cargo) are ubiquitinated in their cytosolic parts by attachment of Lys63-linked polyubiquitin chains, which then serve as a signal for subsequent sorting and delivery of cargo to lysosomes via the multivesicular bodies (MVB) pathway.[30,31] Lys63-linked polyubiquitin chains attached to receptors are required for their binding to the ESCRT machinery, whose members shuttle the cargo and package it into intraluminal vesicles (ILVs) in MVBs (endosomes carrying ILVs are known as MVBs). The ESCRT members appear to play distinct roles in this sorting process. ESCRT-0 clusters ubiquitinated cargo on early endosomes and subsequently passes it to the next member, ESCRT-I, which is responsible for recruiting ESCRT-II. ESCRT-I and -II work in tandem to bend the membrane, creating membrane buds, while ensuring that the cargo is confined to these newly formed buds. In the final step of cargo sorting, components of ESCRT-III assemble at bud necks to catalyze the scission process, whereby the newly formed vesicles carrying cargo are released into the lumen of the endosome.[29,31−33] Subsequently, these newly formed ILVs fuse with the lysosome, delivering the cargo for its destruction. It is important to note that the cargo is deubiquitinated prior to its sequestration into ILVs to spare ubiquitin from being destroyed in the process. Accordingly, certain members of ESCRT-III

feature binding domains for recruiting AMSH and USP8 (also known as UBPY), the two mammalian DUBs known to regulate endocytic sorting.[30,31,34−36] It is not clear why two DUBs, one exquisitely specific for the Lys63-linked polyubiquitin chain (AMSH) and the other with no specificity (USP8), are chosen for this task. Interestingly, in mammals, the initial complex, ESCRT-0, can also recruit both DUBs, the functional significance of which remains to be elucidated.[37] One possibility is that recruitment of AMSH might be required for shortening polyubiquitin chains, so that the cargo can be passed easily from ESCRT-0 to ESCRT-I and -II, a necessity arising because the latter two complexes manifest affinity for the polyubiquitin chain weaker than that of ESCRT-0. The chain shortening action of AMSH is consistent with its high selectivity for Lys63-linked chains; it can disassemble Lys63-linked chains but perhaps cannot remove ubiquitin completely from the cargo. In contrast, the recruitment of USP8 at the ESCRT-0 stage might lead to complete deubiquitination of the cargo, resulting in its falling off from the ESCRT complexes. This would likely facilitate its recycling back to the plasma membrane.[37,38]

Our laboratory has been interested in understanding the role AMSH plays at the ESCRT-0 stage in regulating endocytic sorting. So far, we have determined the structure of AMSH and established a mechanism of its activation upon binding to the STAM component of ESCRT-0. Specifically, using site-directed mutants, we have shown recently that the UIM domain of STAM, abutting its SH3 domain that it uses to bind to AMSH, could facilitate catalysis by binding to the proximal ubiquitin of a diubiquitin substrate.[38] (In diubiquitin, a lysine residue of one ubiquitin, called the proximal ubiquitin, is covalently attached to the last carboxylate group, Gly76, of the other ubiquitin, called the distal ubiquitin.) Such a mode of binding could lead to catalytic activation of the DUB upon its association with ESCRT-0. We wish to provide structural data in support of the biochemical evidence with the hopes of clearly establishing the mechanism underlying the recruitment and activation of AMSH at ESCRT-0. For this reason, we purified a ternary complex consisting of a catalytically inactive construct of Sst2, the *Schizosaccharomyces pombe* orthologue of AMSH, the UIM-SH3 construct representing STAM, and the Lys63-linked diubiquitin substrate with the aim of crystallizing it. Although we are yet to crystallize the ternary complex, our efforts in this direction so far have yielded cocrystal structures of the enzyme bound to diubiquitin, its substrate, and bound to ubiquitin, its product. Our structural analysis provides important insights into the mode of substrate recognition and shows that one of the products of the diubiquitin substrate, that is the distal ubiquitin, can remain tightly bound to the enzyme after the hydrolysis reaction, as the carboxylate group of ubiquitin's Gly76 is coordinated to the active-site metal and is also hydrogen-bonded with the conserved glutamate that is used for holding the nucleophilic water. These product specific interactions appear to offset the contribution of the proximal ubiquitin in a diubiquitin substrate, thus explaining the close correspondence between the affinity for the product and that for the substrate (the dissociation constant with ubiquitin rivals the Michaelis constant, K_M, for the Lys63-linked diubiquitin substrate). It is thus likely that the cytosolic form of AMSH, and by extrapolation similar JAMM DUBs, would be bound to ubiquitin and exist in an inhibited state.

■ METHODS

Cloning, Expression, and Purification. Full length Sst2 and the UIM-SH3 domains of HseI (STAM orthologue of *S. pombe*) were amplified by polymerase chain reaction using the *S. pombe* cDNA library (a kind gift from K. Gould, Vanderbilt University, Nashville, TN). The catalytic domain of Sst2 (residues 245−435), here termed Sst2^{cat}, and a longer construct of Sst2 (residues 221−435) containing the putative SH3 binding motif (SBM), here termed Sst2$^{\Delta 220}$, were both subcloned into pGEX-6P1 vectors using standard cloning protocols. The DNA encoding the UIM-SH3 domains of HseI was subcloned into the pGEX-6P1 vector. Human ubiquitin was also subcloned into a pGEX-6P1 vector. The resulting recombinant DNA constructs were transformed into *Escherichia coli* Rosetta cells to be expressed as a recombinant protein fused with a glutathione *S*-transferase (GST) tag at their N-termini and purified as described. Six liters of Luria-Bertani cultures was grown at 37 °C until the optical density at 600 nm reached 0.4−0.6 and then induced with 0.1−0.3 mM isopropyl β-D-thiogalactoside (IPTG) to allow overexpression of the protein at 18 °C overnight. The next day, the cells were centrifuged at 8630g for 10 min at 4 °C and the pellets were resuspended in phosphate-buffered saline (PBS) containing 400 mM KCl. Lysozyme was added to the suspension, which was then lysed via a French press. The lysate was centrifuged at 22000g for 45 min at 4 °C to remove the cellular debris. The supernatant was further clarified by centrifugation again at 100000g for 30 min at 4 °C. The GST-tagged protein was purified using a glutathione-Sepharose column (GE Biosciences) according to the manufacturer's protocol. After removal of the GST tag with PreScission protease (GE Biosciences), the protein was further purified by size exclusion chromatography (SEC) in a buffer consisting of 50 mM Tris-HCl, 50 mM NaCl, and 1 mM DTT (pH 7.6) using a Superdex S75 column (GE Biosciences). All protein samples were concentrated, and the final concentrations were measured spectrophotometrically at 280 nm. Samples were flash-frozen and stored at −80 °C until they were used.

Glu286Ala, Asp354Ala, and Thr319Ile mutations were introduced individually into the Sst2^{cat} construct by site-directed mutagenesis following the standard protocol. Additionally, the Glu286Ala, Asp354Ala, Tyr234Val, Thr235Asp, and Glu239Lys point mutations were all introduced sequentially into the Sst2$^{\Delta 220}$ construct (this construct therefore contains five mutations). The presence of these mutations was confirmed by DNA sequencing. The resulting GST-tagged mutants were expressed in *E. coli* and purified following the purification methods described above.

To avoid issues that may arise as a result of an N-terminal pentapeptide cloning artifact from ubiquitin prepared via GST affinity chromatography, ubiquitin was prepared from a pRSETA plasmid (gift from P. Loll, Drexel University, Philadelphia, PA) for isothermal titration calorimetry experiments. After cells had been induced with 300 μM IPTG at an OD$_{600}$ ranging from 0.4 to 0.6, expression was conducted overnight at 18 °C. Cells were harvested at 3570g, and pellets were resuspended in 50 mM sodium acetate (pH 4.5). The suspension was lysed via two rounds of a French press, and the lysate was heated to 80 °C for 5 min before centrifugation at 100000g for 1 h. The lysate was loaded onto a column containing SP-Sepharose Fast Flow resin (GE Healthcare), pre-equilibrated in 50 mM sodium acetate (pH 4.5), and ubiquitin was eluted by applying a step gradient with 50 mM sodium

acetate (pH 4.5) and 1 M NaCl. Ubiquitin was further purified by size exclusion chromatography in a buffer consisting of 50 mM Tris (pH 7.6), 50 mM NaCl, and 1 mM DTT using a Superdex S75 column (GE Biosciences).

Lys63-linked diubiquitin was synthesized enzymatically according to published methods[23] using Lys63Arg and Asp77 ubiquitin mutants, with some modifications. Human E1, Uev1a, and Ubc13 and the two mouse ubiquitin mutants were purified separately and then mixed in a reaction buffer containing 80 mM Tris-HCl (pH 7.4), 20 mM ATP, 20 mM MgCl$_2$, and 1 mM DTT. The reactions were conducted overnight at 37 °C and quenched at room temperature with a 10-fold excess of buffer A [50 mM sodium acetate (pH 4.5)]. To separate synthesized diubiquitin from unreacted ubiquitin, the quenched reactions were loaded onto a MonoS cation exchange column (GE Healthcare) pre-equilibrated with buffer A and eluted using a linear gradient with buffer B [50 mM sodium acetate (pH 4.5) and 1 M NaCl]. Diubiquitin was concentrated and stored at −80 °C until it was used. For one of our crystallography experiments, we also used a form of Lys63-linked diubiquitin that was obtained by semisynthesis.[39]

Crystallization and Data Collection. Crystallization was performed by sitting drop vapor diffusion at room temperature. Crystals of Sst2^{cat} were grown from the mother liquor containing 0.2 M ammonium phosphate dibasic (pH 8.0) and 20% (w/v) poly(ethylene glycol) 3350, with either 2.7% (w/v) 1,6-hexanediol or 91 mM glycine included as an additive. With the help of one of these additives, the crystals attain their maximal size in 1−5 days. Crystals of Sst2^{cat}T319I grew in 1 week in 0.03 M citric acid, 0.07 M bis-tris propane (pH 7.6), 20% PEG 3350, and 1.8% benzamidine hydrochloride (additive).

To prepare a complex of Sst2 and ubiquitin, Sst2^{cat} and ubiquitin were mixed in a ratio of 1:1.6. Crystals of the complex, here termed Sst2^{cat}−Ub, formed at room temperature in 1 week in 0.2 M sodium citrate tribasic dehydrate (pH 8.3) and 20% (w/v) PEG 3350. Sst2^{cat}−Ub also crystallized in 60 days in 0.02 M zinc chloride and 20% (w/v) PEG 3350 (pH 4.5). With the goal of forming a complex between Sst2 and diubiquitin, Sst2^{cat}E286A and Lys63-linked diubiquitin (synthesized artificially by E. Strieter, University of Wisconsin—Madison) were mixed in a ratio of 1.5:1 to form the complex. Crystallization was performed by sitting drop vapor diffusion at room temperature, and crystals grew in 3 days from the mother liquor containing 0.2 M ammonium phosphate dibasic (pH 8.0) and 20% (w/v) PEG 3350. Sst2^{cat}D354A and ubiquitin were also mixed in a ratio of 1.8:1 to make the complex. Crystals of the complex, here termed Sst2^{cat}D354A−Ub, also formed at room temperature in 1 week in 1% (w/v) tryptone, 0.05 M HEPES sodium (pH 7.0), and 20% (w/v) PEG 3350.

The three-protein complex consisting of Sst2$^{\Delta 220}$, the UIM-SH3 domain of HseI, and Lys63-linked diubiquitin (K63-Ub$_2$) was buffer exchanged into 50 mM Tris (pH 7.6), 50 mM NaCl, and 1 mM DTT. The three-protein complex was formed by first mixing Sst2$^{\Delta 220}$ and the UIM-SH3 domain from HseI to form an initial complex, which was purified by size exclusion chromatography on a Superdex S75 column (GE Biosciences). Fractions from the sodium dodecyl sulfate−polyacrylamide gel electrophoresis (SDS−PAGE) gel corresponding to the Sst2−UIM-SH3 complex were pooled, concentrated, and complexed with enzymatically synthesized K63-Ub$_2$. This three-protein complex was then purified by size exclusion chromatography, again on a Superdex S75 column (GE Biosciences). SDS−

PAGE fractions corresponding to the three-protein complex were pooled and concentrated for crystallography. Initial crystallization experiments were performed at 20 °C. A Genomics Solutions Cartesian "Honeybee" 963 crystallization robot was used to set up approximately 700 conditions in a sitting drop format. Large crystals of Sst2 in complex with enzymatically synthesized diubiquitin (Sst2$^{\Delta220}$–K63-Ub$_2$) grew after 1 month at 20 °C from the MCSG-1 crystal screen (Microlytic) mother liquor containing 0.2 M MgCl$_2$, 0.1 M Tris-HCl (pH 8.5), and 25% (w/v) PEG 3350.

Crystals were briefly soaked in a cryoprotectant solution (20−25% ethylene glycol) and flash-frozen by being plunged into liquid nitrogen. Crystals of Sst2^{cat} formed from additive 2.7% (w/v) 1,6-hexanediol were soaked in 2.5 mM zinc chloride for 45 min and washed with 25% ethylene glycol, which was also used as the cryoprotectant. Finally, the crystals were flash-frozen in liquid nitrogen. X-ray diffraction data for Sst2^{cat}, Sst2^{cat}–Ub, and Sst2$^{\Delta220}$–K63-Ub$_2$ were collected at 100 K using a Mar300 CCD detector at beamline 23-ID-D, and diffraction data for Sst2^{cat}T319I and Sst2^{cat}E286A−Ub were collected at 100 K using a Mar300 CCD detector at beamline 23-ID-B at the Advanced Photon Source at Argonne National Laboratory (Argonne, IL). All data were processed with HKL3000.[40]

Structure Determination and Refinement for Sst2^{cat} in Its Free Form. Three crystal structures were obtained for Sst2^{cat} in two space groups. The difference in space groups resulted from crystals that formed from different additives in the same mother liquor. Crystals of Sst2^{cat} grown using glycine as an additive crystallized in the $P2_12_12_1$ space group and diffracted to 1.8 Å. Data were collected, and the structure was determined by molecular replacement with MolRep[41] of the ccp4 suite[42] using the catalytic domain of AMSH-LP[23] as a search model. A homology model for the catalytic domain of Sst2 was generated on the basis of the crystal structure of the catalytic domain of AMSH-LP using the SWISS-MODEL homology modeling server.[43] Crystals of Sst2^{cat} grown using 1,6-hexanediol as an additive crystallized in the $P2_1$ space group and diffracted to 1.45 Å. This structure was also determined by molecular replacement (MR) with MolRep[41] using the Sst2^{cat} structure as a search model. Initial refinements of both structures were conducted in Refmac5[44] using rigid body refinement followed by restrained refinement. The model was built using Coot,[45] and subsequent rounds of refinement were conducted in PHENIX,[46,47] yielding R_{crys} and R_{free} values of 20.2 and 23.8%, respectively, for the $P2_12_12_1$ crystal and 16.7 and 19.2%, respectively, for the $P2_1$ crystal. During refinement, TLS[48,49] was also used, with the entire asymmetric unit taken as one group.

Native Sst2 coordinates two metals, one in the active site and one serving a structural role away from the active site. Using crystals of Sst2^{cat} belonging to the $P2_1$ space group, a fluorescence edge scan was run to detect zinc in the crystal, and data were collected at a wavelength of 1.283 Å. The crystal diffracted to 1.67 Å, and the structure was determined using zinc single-wavelength anomalous dispersion (Zn-SAD). Experimental phasing was performed with AutoSol[50] in the PHENIX suite,[45,46] using Phaser[51] to calculate experimental phases and RESOLVE[52] for density modification and initial model building, yielding interpretable density in the experimental map. Subsequent rounds of model building and refinement were conducted in Coot[45] and PHENIX,[46,47] respectively, yielding R_{crys} and R_{free} values of 17.7 and 21.1%,

respectively. TLS Motion[47,48] was used during refinement, using one group.

Crystals of the MIC-CAP mutant, Sst2^{cat}T319I, belong to the $P2_1$ space group and diffracted to 1.9 Å resolution. Data were collected, and the structure was determined by MR with MolRep[41] using the structure of Sst2^{cat} as the search model. After initial rigid body and restrained refinement with Refmac5,[43] additional rounds of refinement and model building were conducted as described above, yielding R_{crys} and R_{free} values of 18.9 and 21.6%, respectively.

Structure Determination and Refinement of Sst2^{cat}– Ub-Bound Structures. Sst2^{cat} bound to ubiquitin (Sst2^{cat}– Ub) crystallized in two different space groups, arising from different crystallization conditions. The crystal obtained from 0.2 M sodium citrate tribasic dihydrate and 20% (w/v) PEG 3350 (pH 8.3) crystallized in the $P2_1$ space group and diffracted to 1.97 Å resolution. After detection of zinc by running a fluorescence edge scan, data were collected at a wavelength of 1.281 Å using Zn-SAD. The structure was determined as described above, using AutoSol[50] to generate an experimental map with interpretable density, allowing cycles of model building and refinement using Coot[45] and PHENIX,[46,47] respectively. The final model yielded R_{crys} and R_{free} values of 17.7 and 20.7%, respectively. Crystals of Sst2^{cat}–Ub grown in 0.02 M zinc chloride and 20% (w/v) PEG crystallized in the $P2_12_12_1$ space group and diffracted to 1.63 Å resolution. Data were collected, and this structure was determined by MR with MolRep[41] using the Zn-SAD-determined Sst2^{cat}–Ub structure as a search model. The model was initially refined in Refmac5[43] using rigid body followed by restrained refinement. Rounds of model building and refinement in Coot[45] and PHENIX[46,47] gave R_{crys} and R_{free} values of 19.5 and 21.5%, respectively. TLS[48,49] was used, with one group, during refinement of both structures.

Crystals of Sst2^{cat}E286A−Ub, which crystallized in the $P2_12_12_1$ space group, and Sst2^{cat}D354A−Ub, which crystallized in the $P2_1$ space group, diffracted to 1.74 and 2.05 Å resolution, respectively. These structures were also determined by MR using the previously described Zn-SAD-determined Sst2^{cat}–Ub structure as a search model. MR, followed by rounds of refinement and model building, was conducted as described above. The final models yielded R_{crys} and R_{free} values for the E286A mutant bound to ubiquitin of 20.3 and 23.2%, respectively, while the R_{crys} and R_{free} values for the D354A mutant bound to ubiquitin were 20.5 and 25.3%, respectively.

Structure Determination and Refinement of Sst2$^{\Delta220}$– K63-Ub$_2$. Crystals of Sst2$^{\Delta220}$–K63-Ub$_2$, which crystallized in the $P2_12_12_1$ space group, diffracted to 2.3 Å resolution, and the structure was determined by MR using MolRep[41] of the ccp4 suite[42] using a model generated by superposition of Sst2^{cat} with the structure of AMSH-LP bound to diubiquitin (PDB entry 2ZNV[23]) as the search model. After superposition of the structures, AMSH-LP atoms were removed, leaving a model of Sst2 bound to diubiquitin. The model was built using Coot[45] and refined using Refmac5,[44] yielding R_{crys} and R_{free} values of 21.3 and 26.3%, respectively. TLS[48,49] was used during structure refinement in which one group was selected for chain A (Sst2), five groups were selected for chain B (distal ubiquitin), and three groups (proximal ubiquitin) were selected for chain C. Optimized weighting was also applied during structure refinement. All figures for all structures described were rendered with PYMOL (version 1.7.0.0).[53]

Determination of Kinetic Parameters. The kinetic parameters were determined as described previously.[20] Briefly, the enzyme (25 nM Sst2^{cat} or 1.25 μM T319I mutant) was incubated in reaction buffer [50 mM Tris-HCl (pH 7.0), 20 mM KCl, 5 mM MgCl$_2$, and 1 mM DTT] with four concentrations of diubiquitin, ranging from 20 to 100 μM. To elucidate initial rate measurements, these reactions were conducted at 20 °C for 7.5 min (wild type) or 15 min (T319I mutant). We attempted to obtain initial velocity measurements for the E286A mutant, but no activity was detected under these conditions. The reactions were quenched by the addition of 5× SDS−PAGE sample buffer. Because of ubiquitin aggregation upon boiling, samples were not boiled prior to being loaded on an SDS−PAGE gel. Bands corresponding to monoubiquitin were integrated using ImageJ.[54] Ubiquitin standards ranging from 6 to 40 μM were used to draw calibration plots, which were used to quantify the amount of ubiquitin produced via the cleavage of diubiquitin. All kinetic data were analyzed using Kaleidagraph and fit to the Michaelis−Menten equation $V_i = (V_{max}[S])/(K_M + [S])$.

Isothermal Titration Calorimetry. Isothermal titration calorimetry (ITC) experiments were conducted at 25 °C to determine the binding affinity of Sst2 with ubiquitin and diubiquitin using a GE/MicroCal ITC$_{200}$ calorimeter. The protein solutions were dialyzed overnight in 50 mM Tris-HCl (pH 7.6) and 50 mM NaCl, exchanging the buffer three times. A typical experiment consisted of titrating 0.4−1 mM ubiquitin (mono or di) into a 40−50 μM protein solution. A total of 28 injections (1.4 μL/injection) were performed over the course of an experiment. Each experiment had a spacing of 180 s between injections that allows for a return to baseline before the subsequent injection. The data were baseline corrected by NITPIC[55] and analyzed using a one-site model from SEDPHAT.[56]

■ **RESULTS**

Isolation of a Sst2−UIM-SH3 Domain−Lys63-Linked Diubiquitin Ternary Complex. We have previously shown that an AMSH construct spanning its DUB domain and its N-terminally adjacent SH3 binding motif (SBM) can be activated by the UIM-SH3 construct of the ESCRT-0 member STAM.[38] To characterize the underlying activation mechanism structurally and to gain insights into the mode of recruitment of AMSH to ESCRT-0, we aimed to crystallize the ternary complex consisting of a catalytically inactive DUB domain construct of AMSH (bearing the active-site Glu to Ala mutation), UIM-SH3, and Lys63-linked diubiquitin. However, we were unable to crystallize this ternary complex, or even the binary complex of AMSH with diubiquitin. We then turned to Sst2, the *S. pombe* orthologue of AMSH. Catalytic constructs of Sst2 (Figure 1), including many of its mutants, showed better expression and appeared to be suitable for crystallization (the construct alone and its mutants readily yielded crystals from multiple conditions). To generate the corresponding ternary complex with the *S. pombe* constructs, we prepared a similar inactivating mutant of the enzyme by replacing the active-site Glu with Ala and prepared a complex with Lys63-linked diubiquitin. Crystallization trials of this binary complex yielded crystals, but surprisingly, these crystals happened to be those of Sst2 bound to ubiquitin, a product fragment of diubiquitin. Thus, in contrast to our expectation that the active-site Glu to Ala mutant would be inactive, as has been seen in other thermolysin-like proteases,[57,58] there was enough hydrolytic
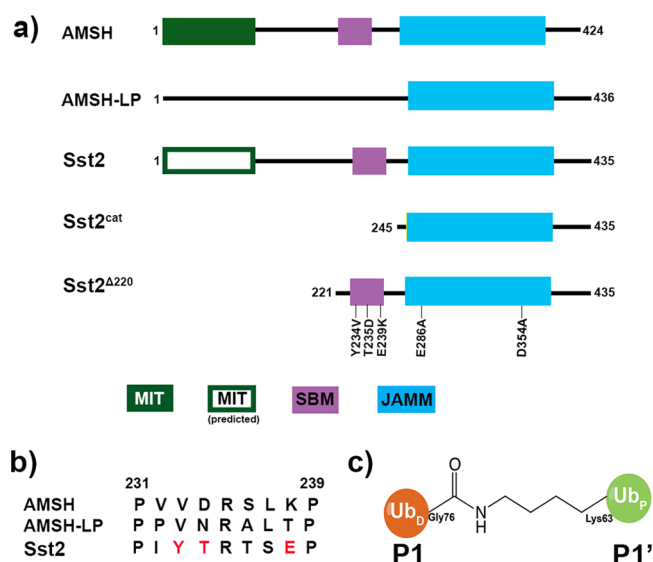

Figure 1. Comparison of AMSH, AMSH-LP, and Sst2. (a) Domain structures of AMSH, AMSH-LP, and Sst2. The JAMM domain is colored blue, while the SBM and MIT domains are colored purple and green, respectively. Sst2^{cat} and Sst2^{Δ220} were used to crystallize product- and substrate-bound structures, respectively. Sst2^{Δ220} contains mutations that both inactivated the enzyme (for substrate binding) and knocked in a functional SBM for recognition of the SH3 domain of STAM. (b) Comparison of the SBM of AMSH, AMSH-LP, and Sst2. Mutations made in the SBM of Sst2 to make it functional for SH3 binding are colored red. (c) The isopeptide bond of diubiquitin is formed between proximal ubiquitin (UbP), which donates its lysine, and distal ubiquitin (UbD), which donates its C-terminal carboxylate group. In other protease systems, UbD and UbP are equivalent to the P and P′ fragments, respectively, of a peptide bond.

activity under the crystallization conditions to cleave diubiquitin, leading to cocrystallization with the product (see below). To completely inactivate the enzyme so that it could form a stable complex with the diubiquitin substrate and the UIM-SH3 construct, we had to introduce an additional mutation by changing an active-site zinc-coordinating Asp to Ala. Furthermore, Sst2, while sharing a high level of sequence similarity with AMSH in both its catalytic and MIT (microtubule interacting and trafficking) domain (for binding to ESCRT-III members), bears three substitutions in its corresponding SBM that are presumed to render the SBM nonfunctional for binding to the SH3 domain of STAM (Hse1 in *S. pombe*). We therefore engineered three mutations in this domain (Figure 1) to restore a functional SBM as found in the human counterpart (see below), with the hope of creating a construct of Sst2 that would bind to the UIM-SH3 domain of Hse1. Indeed, a ternary complex consisting of the catalytically inactive Sst2 DUB construct, Lys63-linked diubiquitin, and the UIM-SH3 domain could be purified via size exclusion chromatography, indicating that a stable complex was formed among the three proteins (Figure 1 of the Supporting Information). Despite several attempts to conduct crystallization trials, the complex so far has yielded crystals of only the enzyme bound to Lys63-linked diubiquitin. The crystal structures of these two complexes allow comparison of Sst2 bound to the product, generated, as described previously, *in situ* from a mixture of enzyme (catalytically impaired because of the Glu to Ala mutation, yet with some residual activity) and its substrate. Additionally, we decided to take advantage of Sst2's

Table 1. Crystallographic Data Collection and Refinement Statistics for the Catalytic Domain of Sst2

	Sst2^{cat}	Sst2^{cat}−Zn Edge	Sst2^{cat}
		Data Collection[a]	
space group	$P2_1$	$P2_1$	$P2_12_12_1$
cell dimensions			
a, b, c (Å)	56.1, 69.4, 62.0	56.2, 69.4, 61.9	54.8, 58.1, 187.5
α, β, γ (deg)	90.0, 104.8, 90.0	90.0, 104.7, 90.0	90.0, 90.0, 90.0
wavelength (Å)	1.033	1.283	1.033
resolution (Å)	50.0−1.45 (1.48−1.45)	50.0−1.67 (1.70−1.67)	50.0−1.80 (1.83−1.80)
R_{merge}[b] (%)	6.0 (68.5)	7.2 (51.4)	8.7 (62.8)
$I/\sigma I$	19.3 (2.02)	20.8 (3.5)	17.8 (2.9)
completeness (%)	99.7 (99.2)	96.9 (90.9)	97.9 (96.6)
redundancy	3.8 (3.7)	7.7 (7.2)	6.0 (6.1)
		Refinement	
resolution (Å)	1.45	1.67	1.80
no. of reflections	80642	51582	55256
R_{work}[c]$/R_{free}$[d]	16.7/19.2	17.7/21.1	20.2/23.8
no. of atoms			
protein	3017	2981	4436
ion	4	4	6
water	212	268	217
rmsd			
bond lengths (Å)	0.007	0.006	0.008
bond angles (deg)	1.260	1.120	1.143
Ramachandran plot			
preferred (%)	97.7	98.6	97.3
allowed (%)	1.9	1.1	2.3
disallowed (%)	0.3	0.3	0.4
average B factor (Å^2)			
protein	26.1	25.8	35.7
ion	21.7	25.4	31.5
water	33.8	34.1	34.4
ligand	38.3	34.7	54.3

[a]Values in parentheses are for the highest-resolution shell. [b]$R_{merge} = \sum\sum|I_{hkl} - I_{hkl(j)}|/\sum\sum I_{hkl}$, where $I_{hkl(j)}$ is the observed intensity and I_{hkl} is the final average intensity. [c]$R_{work} = \sum||F_{obs}| - |F_{calc}||/\sum|F_{obs}|$. [d]$R_{free} = \sum||F_{obs}| - |F_{calc}||/\sum|F_{obs}|$, where R_{free} and R_{crys} are calculated using a randomly selected test set of 5% of the data and all reflections excluding the 5%, respectively.

crystallizability to understand the basis of the MIC-CAP mutation[59] at the atomic level by generating the Thr319Ile mutant in the DUB domain of Sst2.

Structure of the Catalytic Domain of Sst2 in Its Free Form. *Structure Determination.* To gain structural insights into Sst2, we have crystallized a construct spanning the catalytic domain of the protein, here termed Sst2^{cat} (residues 245−435). Sst2^{cat} crystallized in two different space groups, $P2_1$ and $P2_12_12_1$. The $P2_1$ form has two subunits in the asymmetric unit, whereas the $P2_12_12_1$ form has three subunits. The structure of Sst2^{cat} was determined by zinc single-wavelength anomalous dispersion (SAD) and also by molecular replacement (MR) using the structure of the catalytic domain of AMSH-LP as the search model[23] (see Table 1 for crystallographic data collection and refinement statistics). The structures were refined yielding satisfactory crystallographic and free R factors with good stereochemistry.

Like the DUB domain of AMSH-LP and AMSH,[20,23] its two most closely related homologues, the structure of Sst2^{cat} features a JAMM core with two characteristic insertions, insertion 1 (Ins-1, residues 308−333) and insertion 2 (Ins-2, residues 388−413). These insertions play an important role in ubiquitin recognition and contribute key functional groups for catalysis performed by these enzymes. The JAMM core consists of a mixed β-sheet, which adopts the shape of a partially open

β-barrel sandwiched by two α-helices, one on top (α1) and one on the bottom (α3) (Figure 2a), an architectural feature shared among the members of JAMM domain proteins, such as *Af*JAMM and Prp8.[18,60−63] As seen in AMSH-LP and AMSH, the catalytic site is lined mostly by residues from the JAMM core, from the loop between α1 and β2, α3, β6, and the loop following it (Figure 2a). The catalytic zinc is held in tetrahedral geometry by residues from the JAMM core, coordinated by His341, His343 (located on β6 and immediately following it), Asp354 (located on α3), and a water molecule that is hydrogen bonded to Glu286 (located on the loop segment following α1) (Figure 2b). This zinc site is complemented by the conserved serine residue on α3 (Ser351), which serves as the oxyanion-stabilizing side chain. The second, structural zinc is located approximately 14 Å from the active-site zinc and is coordinated by the residue His356 from the JAMM core and residues His404, His406, and Cys397 from Ins-2 (Figure 2c), the same set of equivalent residues that coordinate the second zinc ion in AMSH-LP and AMSH.

The structure of Sst2 can be superimposed with those of AMSH and AMSH-LP with Cα root-mean-square deviations (rmsds) of 0.71 and 0.59 Å, respectively, indicating substantial structural conservation between these JAMM DUBs. A noteworthy difference, however, is the presence of a cis peptide unit in Sst2, Asp387-Pro388. The cis conformation permits the
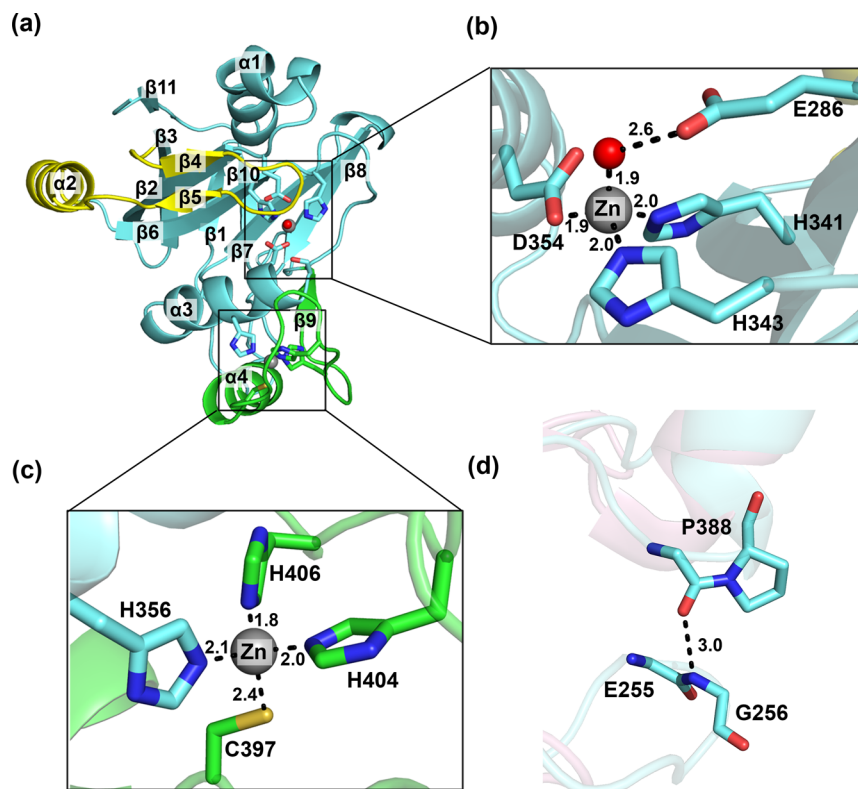
Figure 2. Structure of the catalytic domain of Sst2. (a) Ribbon diagram representing secondary structures of Sst2^{cat}. The JAMM core, Ins-1, and Ins-2 of Sst2 are colored aquamarine, yellow, and green, respectively. The insets show the active-site zinc and the structural zinc. (b) Expanded view of zinc coordination in the active site. Zinc binds the His-His-Asp motif of Sst2 and one water molecule in a tetrahedral coordination. (c) Expanded view of the structural zinc coordination site, located 14 Å from the catalytic center. (d) Cis peptide conformation of Pro388 in Sst2 (aquamarine) forming a hydrogen bond with backbone NH groups of Gly256. AMSH is colored pink for reference.

carbonyl group of Pro388 to engage in a hydrogen bond with the backbone NH group of Gly256, from the turn segment of the N-terminal β-hairpin of Sst2^{cat} (Figure 2d). The significance of the cis peptide unit is unclear at the moment. Perhaps such hydrogen bonding could provide extra stability to the helix starting from Pro388, a helix that contributes a critical cysteine (Cys397) for holding the structural zinc in position.

Structure of the Complex with Lys63-Linked Diubiquitin. Crystallization of Sst2 and Lys63-linked diubiquitin (K63-Ub$_2$) was accomplished by using an Sst2 construct, termed Sst2$^{\Delta220}$, which spans residues 221−435 and was designed to contain the SBM motif from AMSH by incorporation of three point mutations: Tyr234Val, Thr235Asp, and Glu239Lys. To prevent the cleavage of diubiquitin, we also introduced two mutations into the active site; Glu286, which binds to the nucleophilic water, and Asp354, which coordinates the catalytic zinc, were both mutated to alanine, resulting in an inactive form of Sst2 [unlike the Glu286Ala mutant alone, which exhibited residual activity (see below)]. As described before, crystals containing the complex of Sst2$^{\Delta220}$ and K63-Ub$_2$ formed from a mixture purified via gel filtration chromatography comprising Sst2$^{\Delta220}$, the UIM-SH3 domain from HseI, and K63-Ub$_2$. It is likely that K63-Ub$_2$ forms a tight complex with Sst2, as indicated by ITC measurements with a catalytically inactive mutant, revealing a K_D of 1.1 ± 0.1 μM (Table 6), whereas the UIM-SH3 construct may have somewhat weaker affinity for the binary complex, which could explain why we are unable to crystallize the ternary complex. The structure was determined by molecular replacement using a model of Sst2−K63-Ub$_2$ generated by

superimposition of Sst2^{cat} with the structure of AMSH-LP bound to K63-Ub$_2$ (PDB entry 2ZNV[23]) and refined yielding satisfactory crystallographic, free R factors and good stereochemistry (Table 2). The 27 N-terminal residues (221−247) of Sst2$^{\Delta220}$ were not resolved in the crystal structure. Moreover, because of a lack of side-chain density, the final model has alanine substitutions of the following residues in Sst2: Phe248, Lys249, Glu297, Asn331, and Val434. Furthermore, poor density in chain C (proximal ubiquitin), presumably resulting from positional disorder (Figure 2 of the Supporting Information), forced us to delete residues 7−11, 28−42, 47, and 70−76 from chain C.

The overall three-dimensional fold of Sst2$^{\Delta220}$−K63-Ub$_2$ is highly similar to the structure of the DUB domain of AMSH-LP bound to K63-Ub$_2$ (PDB entry 2ZNV) with an rmsd of 1.19 Å of Cα atoms over 266 residues from both Sst2 and K63-Ub$_2$. K63-Ub$_2$ binds to Sst2$^{\Delta220}$ in an extended conformation around the isopeptide linker (Figure 3a), with the majority of the protein contacts contributed by the distal ubiquitin (Figure 3c), consistent with the mode of diubiquitin binding observed in AMSH-LP. Comparison of the buried surface areas for distal and proximal ubiquitin using PISA,[64] 1120 and 426 Å^2, respectively, further augments this observation. Sst2$^{\Delta220}$ features a catalytic channel spanning approximately 20 Å, occupied largely by the C-terminal tail of the distal ubiquitin, allowing proper orientation of the isopeptide bond in the active site. The active site of Sst2 normally coordinates zinc, but our structure is in the apo (unmetalated) state, because of two mutations in residues contributing to zinc coordination: mutation of Asp354 to alanine has a direct impact on metal

Table 2. Crystallographic Data Collection and Refinement Statistics for the Catalytic Domain of Sst2 Bound to Ubiquitin or Diubiquitin

	Sst2^{cat}–Ub	Sst2^{cat}–Ub	Sst2$^{\Delta 220}$–K63-Ub$_2$
	Data Collection[a]		
space group	$P2_1$	$P2_12_12_1$	$P2_12_12_1$
cell dimensions			
a, b, c (Å)	71.2, 57.0, 81.2	57.3, 74.6, 139.3	49.5, 56.7, 135.1
α, β, γ (deg)	90.0, 104.6, 90.0	90.0, 90.0, 90.0	90, 90, 90
wavelength (Å)	1.281	1.033	1.033
resolution (Å)	50.0–1.97 (2.0–1.97)	50.0–1.63 (1.66–1.63)	60.0–2.30 (2.34–2.30)
R_{merge}[b] (%)	13.9 (90.0)	12.2 (92.6)	11.2 (54.9)
$I/\sigma I$	20.9 (3.5)	17.1 (2.3)	34.5 (4.1)
completeness (%)	98.7 (97.6)	99.8 (96.1)	100.0 (100.0)
redundancy	7.5 (7.0)	7.3 (7.0)	6.8 (6.7)
	Refinement		
resolution (Å)	1.97	1.63	2.30
no. of reflections	44008	74731	16689
R_{work}[c]/R_{free}[d]	17.7/20.7	19.5/21.5	21.3/26.3
no. of atoms			
protein	4108	4200	2396
ion	4	8	1
water	304	227	52
rmsd			
bond lengths (Å)	0.007	0.006	0.007
bond angles (deg)	1.101	1.112	1.183
Ramachandran plot			
preferred (%)	98.0	98.3	98.7
allowed (%)	1.8	1.7	1.3
disallowed (%)	0.2	0.0	0.0
average B factor (Å^2)			
Sst2^{cat}	26.5	18.2	19.1
distal ubiquitin	40.9	26.4	18.3
proximal ubiquitin	–	–	14.1
ion	25.6	14.9	23.4
water	35.7	22.9	29.4
ligand	40.8	27.5	37.3

[a]Values in parentheses are for the highest-resolution shell. [b]$R_{merge} = \sum\sum|I_{hkl} - I_{hkl(j)}|/\sum\sum I_{hkl}$, where $I_{hkl(j)}$ is the observed intensity and I_{hkl} is the final average intensity. [c]$R_{work} = \sum||F_{obs}| - |F_{calc}||/\sum|F_{obs}|$. [d]$R_{free} = \sum||F_{obs}| - |F_{calc}||/\sum|F_{obs}|$, where R_{free} and R_{crys} are calculated using a randomly selected test set of 5% of the data and all reflections excluding the 5%, respectively.

affinity, because it is a member of the catalytic triad that coordinates to zinc. Metal affinity is further diminished by an additional mutation, to Glu286, which indirectly coordinates zinc by binding the nucleophilic water. In place of zinc, the active site of Sst2$^{\Delta 220}$–K63-Ub$_2$ contains a water molecule. This structure also reveals an alternative rotameric conformation of Cys288 in Sst2, resulting in the formation of a partially occupied disulfide bond with Cys317 (see below).

Proximal Ubiquitin Recognition. Proximal ubiquitin binding is similar to that observed in the crystal structure of AMSH-LP bound to K63-Ub$_2$. Figure 3d shows the superposition of Sst2$^{\Delta 220}$–K63-Ub$_2$ and AMSH-LP bound to K63-Ub$_2$ (PDB entry 2ZNV[23]). The primary areas of Sst2 contributing to the recognition of proximal ubiquitin stem from the Zn^{2+} coordination loop of Ins-2 and a loop that links helix α3 to strand β6 in the JAMM core. The residues engaged in proximal ubiquitin recognition via van der Waals interactions or hydrogen bonding, are completely conserved between AMSH-LP and AMSH. Phe403 makes three van der Waals contacts with the isopeptide segment of diubiquitin: the Cζ and Cε_2 atoms of Phe403 form van der Waals contacts with the Cδ atom of Lys63 from the proximal ubiquitin (4.1 and 3.9 Å,

respectively), and the Cε_2 atom of Phe403 makes an additional contact with the carbon atom of Gly76 from the distal ubiquitin. Additional hydrophobic contacts with proximal ubiquitin are likewise formed from the Cβ atom of Phe403 and the Cζ atom of Phe349 with the Cγ atom of Gln62 and the Cγ atom of Lys63 from proximal ubiquitin, while Pro405 forms a stacking interaction with Phe4 of the proximal ubiquitin (Figure 3b). Consistent with the AMSH-LP–K63-Ub$_2$ crystal structure, hydrogen bonding interactions from two residues in Sst2, Thr347 and Ser352, also make an important contribution to the recognition of proximal ubiquitin. The Oγ atom and NH from the main chain of Thr347 make hydrogen bonds with the Oε and Nε atoms of Gln62, while both the Oγ atom and main-chain NH of Ser352 form hydrogen bonds with Oγ_2 of Glu64 (Figure 3b).

Earlier mutational studies in both AMSH and AMSH-LP on residues that engage in binding of the proximal ubiquitin found a significant reduction in k_{cat} with a minimal change in K_M as compared to those of the wild-type enzyme, therefore indicating a role for the proximal ubiquitin in the rate-limiting step of catalysis with little involvement in the ground-state interaction with the substrate.[23,38] It is likely that through their
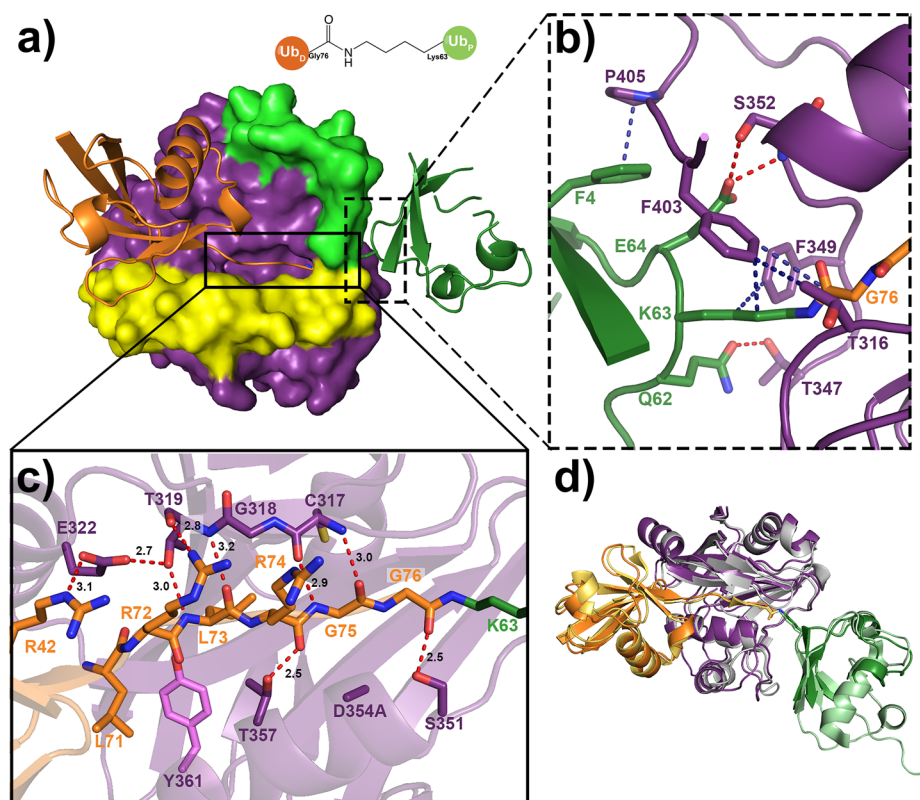
Figure 3. Crystal structure of Sst2 in complex with K63-Ub$_2$. (a) Surface representation of Sst2 (purple) bound to diubiquitin. Proximal ubiquitin is colored dark green, while distal ubiquitin is colored orange. AMSH/Sst2 specific insertions 1 and 2 are colored yellow and green, respectively. (b) Proximal ubiquitin recognition is limited to a few residues. Hydrophobic interactions are shown with blue dashes and hydrogen bonds with red dashes. (c) Distal ubiquitin is held tightly in the active site through a number of mostly hydrogen bonding interactions. (d) Superposition of Sst2 (purple) and AMSH-LP (gray) bound to diubiquitin. Proximal ubiquitin bound to Sst2 is colored dark green and proximal ubiquitin bound to AMSH-LP light green. Distal ubiquitin bound to Sst2 is colored orange and distal ubiquitin bound to AMSH-LP yellow.

interactions with the proximal ubiquitin, these residues play a critical role in properly orienting the isopeptide for Lys63 linkage specific deubiquitination.

Crystallization of Sst2 in Its Product-Bound State. Residual Activity in the Glu286Ala Mutant. To improve our understanding of interactions with Lys63-linked polyubiquitin substrates, we first attempted to cocrystallize the Glu286Ala mutant of Sst2^{cat} with Lys63-linked diubiquitin. The mutation was presumed to render the enzyme inactive on two accounts. (1) Glu286 plays a role in holding the catalytic water in its position allowing it to serve as the fourth ligand for the active-site zinc. Its mutation to Ala is likely to lead to a loss of zinc from the active site.[23,65] With the loss of zinc, there is no water to act as a nucleophile. (2) The glutamate is also presumed to function as both a general base and acid in the hydrolysis reaction, assuming that Sst2 hydrolyzes its substrates following a thermolysin-like mechanism. Quite unexpectedly, the crystals obtained from a solution containing both Sst2^{cat}E286A and Lys63-linked diubiquitin (prepared semisynthetically[39]) proved instead to be those of Sst2^{cat}E286A bound to one ubiquitin moiety occupying the distal site. Thus, this structure yielded a view of the enzyme's product-bound state, in which the product was actually generated from reaction during crystallization trials. Because this product-bound structure contained the E286A mutation in the enzyme, we also cocrystallized Sst2^{cat} with ubiquitin (herein termed the Sst2^{cat}—Ub complex) to visualize product contacts with the wild-type enzyme (resulting in two additional structures of the enzyme bound to its

product). Because the structures share many similarities, we will use the Sst2^{cat}E286A structure to describe the interactions of Sst2 with ubiquitin.

Sst2^{cat}—Ub crystallized in two different space groups, $P2_1$ and $P2_12_12_1$, with two subunits in the asymmetric unit of both crystal forms (Figure 3 of the Supporting Information). The structure of the $P2_1$ form of wild-type Sst2^{cat}—Ub was determined by Zn SAD, and the refined model was used as the search model for determining the structure of both the wild-type protein and the E286A mutant ubiquitin complexes in the $P2_12_12_1$ form (see Tables 2 and 3 for crystallographic data collection and refinement statistics). Interestingly, the subunits in the asymmetric unit of wild-type Sst2^{cat}—Ub in the orthorhombic crystal form show zinc-mediated packing at the interface (Figure 4 of the Supporting Information). Two zinc ions are found at the interface, related by a 2-fold noncrystallographic symmetry. The tetrahedral coordination around these zinc ions is furnished by two His residues from one subunit, a Glu from the symmetry-related partner, and a chloride ion (Figure 4b of the Supporting Information). These zinc-coordinating interactions appear to provide substantial stabilization leading to the packing of the monomers in the crystallographic dimer as observed here. Additional hydrogen bonding interactions (two copies of Ser324-Gln428, each pair contributing two hydrogen bonds) and van der Waals packing of aromatic side chains (Phe328) also contribute to dimer formation. The zinc and chloride ions found at the dimer

Table 3. Crystallographic Data Collection and Refinement Statistics for Catalytic Mutants of Sst2

	E286A−Ub	T319I	D354A−Ub
	Data Collection[a]		
space group	$P2_12_12_1$	$P2_1$	$P2_1$
cell dimensions			
a, b, c (Å)	57.0, 95.3, 112.9	58.1, 74.1, 64.8	42.4, 58.0, 56.2
α, β, γ (deg)	90.0, 90.0, 90.0	90.0, 113.4, 90.0	90.0, 108.9, 90.0
wavelength (Å)	1.033	1.033	1.033
resolution (Å)	50.0−1.74 (1.78−1.74)	50.0−1.90 (1.93−1.90)	60.0−2.05 (2.09−2.05)
R_{merge}[b] (%)	11.6 (86.7)	7.0 (56.5)	8.6 (62.5)
$I/\sigma I$	19.4 (2.7)	18.7 (2.9)	16.8 (2.6)
completeness (%)	100 (100)	100 (100)	100 (100)
redundancy	5.8 (5.5)	3.8 (3.8)	3.8 (3.7)
	Refinement		
resolution (Å)	1.74	1.90	2.05
no. of reflections	63007	39791	16420
R_{work}[c]/R_{free}[d]	19.5/22.5	18.9/21.6	20.5/25.3
no. of atoms			
protein	4130	2911	2042
ion	4	4	1
water	409	164	78
rmsd			
bond lengths (Å)	0.02	0.006	0.008
bond angles (deg)	2.0	1.122	1.213
Ramachandran plot			
preferred (%)	98.0	97.8	95.7
allowed (%)	2.0	1.9	4.3
disallowed (%)	0.0	0.3	0.0
average *B* factor (Å²)			
Sst2^{cat}	22.6	24.7	31.1
distal ubiquitin	25.5	−	29.7
ion	20.2	18.0	29.9
water	29.9	27.8	31.8
ligand	33.6	43.3	33.8

[a]Values in parentheses are for the highest-resolution shell. [b]$R_{merge} = \sum\sum|I_{hkl} - I_{hkl(j)}|/\sum\sum I_{hkl}$, where $I_{hkl(j)}$ is the observed intensity and I_{hkl} is the final average intensity. [c]$R_{work} = \sum||F_{obs}| - |F_{calc}||/\sum|F_{obs}|$. [d]$R_{free} = \sum||F_{obs}| - |F_{calc}||/\sum|F_{obs}|$, where R_{free} and R_{crys} are calculated using a randomly selected test set of 5% of the data and all reflections excluding the 5%, respectively.

interface might have been from the reservoir solution, which contained $ZnCl_2$.

Structures of Sst2^{cat}−Ub (1.6 Å) and Sst2^{cat}E286A−Ub (1.7 Å) provide insights into the product-bound state of the enzyme. Like the distal moiety of the substrate in the diubiquitin-bound structure, ubiquitin as the product is held tightly by a number of intermolecular interactions that include hydrogen bonding, van der Waals contacts, and salt bridges, with most of the interactions contributed by contacts holding its extreme C-terminal hexapeptide LRLRGG motif in the active-site cleft (Figure 4). This hexapeptide segment, as observed in the substrate-bound state, aligns itself at the active-site cleft as an extended β-strand, in register with strand β5 of Ins-1, and is engaged in backbone and side-chain interactions with strand β5 on one side and helix α3 from the JAMM core on the other. Interestingly, the JAMM core residues involved in ubiquitin binding on helix α3 are conserved in AMSH, AMSH-LP, and Sst2, while residues from strand β5 of Ins-1 that contribute to distal ubiquitin recognition are not entirely conserved in all three proteins (Figure 5 of the Supporting Information), suggesting that the JAMM core residues are structurally important while the insertion residues, which evolved later, are more interchangeable.

Generally, ubiquitin-interacting proteins recognize a hydrophobic patch surrounding Ile44 of ubiquitin (the I44 patch).[66−68] Like other cysteine protease DUBs and AMSH-LP, Sst2 also recognizes the I44 patch in the distal ubiquitin. The structures of both ubiquitin and diubiquitin complexes of Sst2 show contacts with residues in this patch, which consists of Leu8, Ile44, Val70, and the Cβ atom of His68 of ubiquitin (Figure 4a). In the case of AMSH-LP, the aliphatic side chains of Val328 and Phe332 in Ins-1 interact with the residues of the hydrophobic patch. However, in both Sst2 and AMSH, Val328 is substituted with Glu322 and Glu316, respectively. The model of AMSH[244] bound to Lys63-linked diubiquitin predicts that Glu316 of AMSH might form electrostatic and polar interactions with Arg42 and Gln49;[20] however, in Sst2, the equivalent residue, Glu322, forms an electrostatic interaction with only Arg42 of ubiquitin. Our structures of ubiquitin- and diubiquitin-bound complexes of Sst2 reveal that Phe326 in Ins-1 makes a number of van der Waals contacts with the residues of the I44 patch, while Gln329 in Ins-1 makes van der Waals contacts with the side chain of Leu8 (Figure 4a). These complex structures also reveal the interactions of Met364 from the JAMM core of Sst2 with Ile36, Leu69, Leu71, and the Cγ atom of Thr7 in the distal ubiquitin, which forms the hydrophobic pocket opposite the I44 patch (Figure 4c).
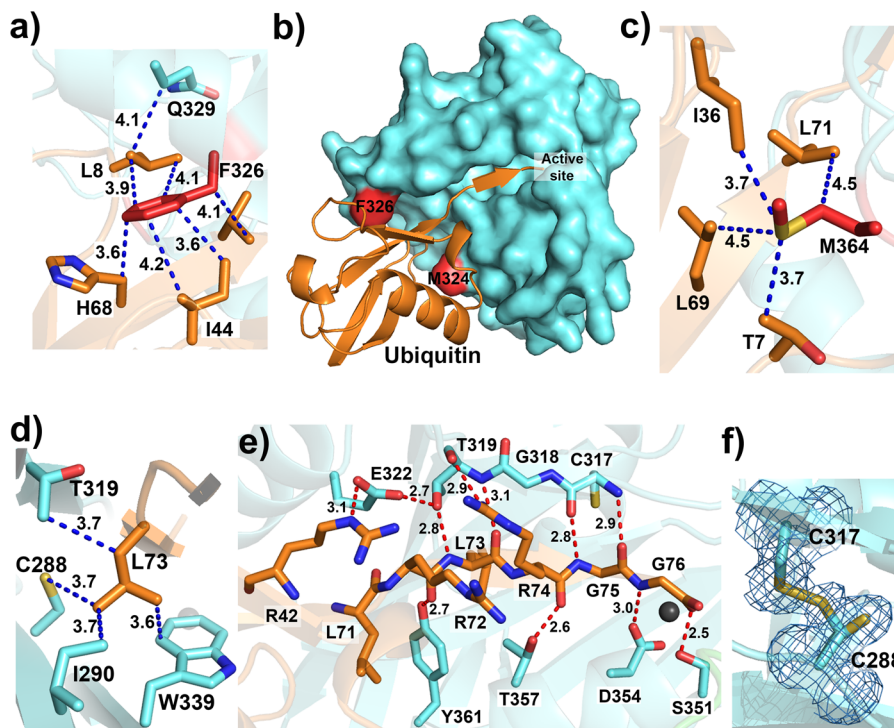
Figure 4. Ubiquitin binding in Sst2. (a) Interactions of Phe326 with the Ile44 hydrophobic patch of ubiquitin. (b) Surface representation of the DUB domain of Sst2 (aquamarine) bound to ubiquitin (orange) highlighting the residues (red) involved in interactions with the hydrophobic patches of ubiquitin. (c) Interactions of Met364 with the residues in the hydrophobic pocket opposite the Ile44 patch. (d) van der Waals interactions of Leu73 of ubiquitin with residues of Sst2 shown with blue dashes. (e) Residues of Sst2 involved in distal ubiquitin recognition. Hydrogen bonds are shown with red dashes. (f) Formation of a potential disulfide bond in Sst2. One of the alternative conformations of Cys288 forms a disulfide bond with Cys317. The disulfide bond-forming residues are outlined by electron density from a $2F_o - F_c$ map contoured at 1.2σ.
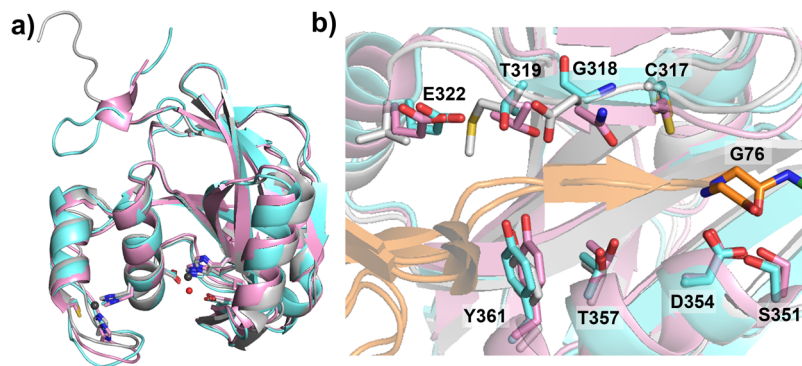
Figure 5. Structural comparison of AMSH, AMSH-LP, and Sst2. (a) Superposition of catalytic domains of AMSH (pink), AMSH-LP (gray), and Sst2 (aquamarine). (b) Superposition of AMSH (pink), AMSH-LP bound to K63-Ub$_2$ (gray), and Sst2^{cat}−Ub (aquamarine) showing the residues involved in the recognition of distal ubiquitin binding. Ubiquitin is colored orange.

Thus, as the foregoing discussion has indicated, many of the interactions seen with the distal ubiquitin in the structure of Sst2$^{\Delta220}$−K63-Ub$_2$ are preserved in the product-bound structure.

Superposition of the DUB domain of AMSH, the AMSH-LP−K63-Ub$_2$ complex, and the Sst2^{cat}E286A−Ub complex reveals that most of the residues involved in distal ubiquitin recognition are conserved (Figure 5a). However, the two substitutions of Thr313 and Glu316 in AMSH and Thr319 and Glu322 in Sst2 in place of Met325 and Val328 in AMSH-LP imply that the catalytic domain of Sst2 shares more similarities with AMSH than AMSH-LP as far as ubiquitin binding is concerned. Comparison to the structures of AMSH and AMSH-LP shows three substitutions in the distal binding site

(Figure 5b). Interestingly, despite these substitutions, the number of interactions with ubiquitin is not significantly altered. For example, substitution of Gly at position 318 of Sst2 in place of Asn in AMSH and Asp in AMSH-LP leads to a loss of hydrogen bonding and salt bridge interaction with Arg74 of ubiquitin, but hydrogen bonding of Arg74 with Thr319 of Sst2 reestablishes this interaction. Overall, these structures show that the distal site is evolutionarily less constrained than the proximal site.

Product Specific Interactions. In the diubiquitin-bound structure, the Cα atom of Gly76 forms a hydrophobic interaction with the Cε_2 atom of Phe403 and is located adjacent to the metal center, showing how the scissile peptide bond in the substrate would be placed adjacent to the
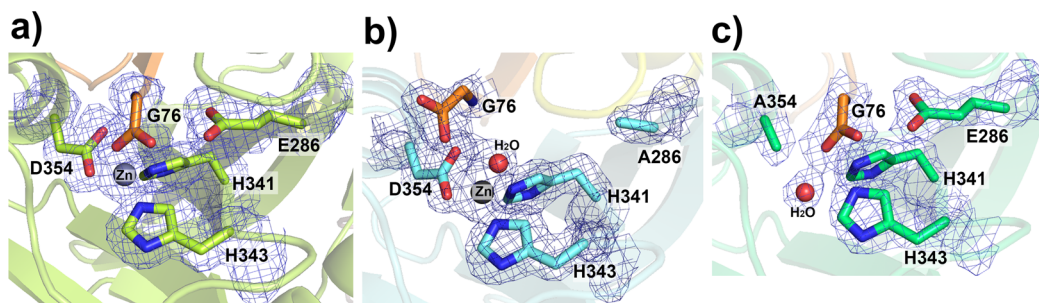
Figure 6. Active sites of Sst2^{cat}, Sst2^{cat}E286A, and Sst2^{cat}D354A bound to ubiquitin. (a) The carboxylate group of Gly76 from distal ubiquitin (P-product fragment) replaces the catalytic water molecule and coordinates with zinc. (b) In Sst2^{cat}E286A, a water molecule is observed in coordination with zinc, displacing the carboxylate group of Gly76. (c) In Sst2^{cat}D354A, water is occupying the zinc site. In all panels, electron density from a $2F_o − F_c$ map is shown as blue mesh (at 1.0σ).

nucleophilic water (Figure 3b). Contrary to our expectation, the hydrolysis of diubiquitin by the E286A mutant means that the active-site water and the metal are still intact in this mutant. Interestingly, the structure of Sst2^{cat}E286A−Ub does reveal zinc in the active site and water coordinating the zinc ion. Some interesting differences can be seen between the E286A product-bound structure and that represented by wild-type Sst2^{cat}−Ub. In the latter, the carboxylate group of Gly76 of ubiquitin coordinates the catalytic zinc to maintain its tetrahedral coordination while also forming a hydrogen bond with Glu286 (Figure 6a). In contrast, the former shows the same carboxylate group displaced from Zn^{2+} by a water that has taken its place in the metal coordination sphere (Figure 6b). This is remarkable because it appears as if we have managed to crystallize a form of the product complex representing a transient solution species in which the product is about to depart and the catalytic water is about to reestablish its contact with the active-site metal.

Although subtle, changes in a loop (flap) located at the top of the active site (near the proximal ubiquitin binding site) could also be observed. The prime residues of interest in this loop are Leu402 and Phe403 (Figure 7a), coming from the Ins-2 segment that also is responsible for coordination of the structural zinc. The loop appears to have moved away from van der Waals contact with Thr316, creating an opening, likely to accommodate the displaced carboxylate in Sst2^{cat}E286A−Ub. This is significant because in all of our other structures (free form, substrate-bound form, and product-bound form in which the C-terminal ubiquitin carboxylate coordinates with zinc), Phe403 and Leu402 make van der Waals contacts with Thr316 and Asp315, resulting in a closed conformation (Figure 7b,c,e). Comparison of the van der Waals contacts made in all four structures is summarized in Table 4.

In Sst2^{cat}−Ub, Phe403 and Thr316 reaching out to one another across the cleft are located 4.0 Å apart, a distance that is close to that of a van der Waals contact between the two. Also contributing to the closed conformation are Leu402 and Thr316, which are 4.4 Å apart, while Phe403 approaches the Cα atom of Gly76 of ubiquitin from the top, making a close van der Waals contact with this residue. In the free form of Sst2^{cat}, the closed conformation at the active-site cleft is maintained in the absence of substrate, as well; however, the mobility of the loop results in Phe403 establishing a contact with Asp315 (instead of Thr316) and Leu402 makes a contact with Thr316. This slight change in interacting partners has completely closed the active-site cleft from the proximal end. Interestingly, the structure of Sst2$^{\Delta 220}$ bound to K63-Ub$_2$ also reveals a closed
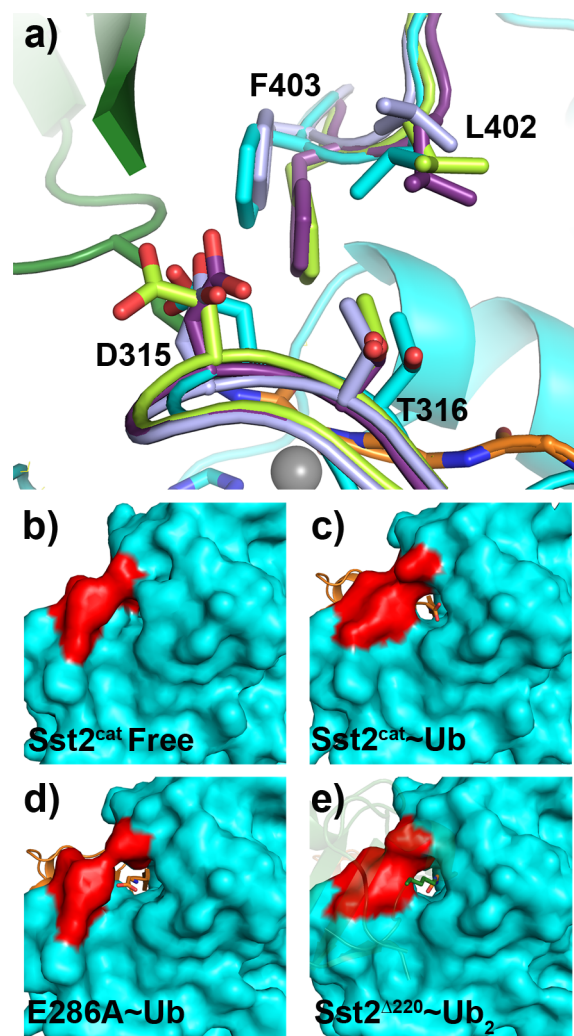

Figure 7. Subtle changes in the loop at the top of the active site (near proximal ubiquitin) appear to open and close the active site. (a) Superposition of our Sst2 structures highlights conformational changes of a loop containing residues Leu402 and Phe403. The free form of Sst2 is colored limon and bound diubiquitin purple, and our two product-bound forms are colored blue-gray (wild-type Sst2) and cyan (E286A). (b−e) Surface representations of Sst2 comparing the position of the loop (red) in all structures.

position of the loop, which makes van der Waals contact with the hydrocarbon portion of the acceptor Lys residue in the proximal ubiquitin. However, this residue, in fact, the two-

Table 4. Comparison of van der Waals Contacts in Residues near the Active Site Indicates That Interactions between Phe403/Leu402 and Thr316 That Result in an Open Form May Play a Role in the Release of the Second Ubiquitin

sample	Sst2^{cat}	Sst2^{cat}–Ub	E286A–Ub	Sst2$^{\Delta 220}$–K63-Ub$_2$
Phe403 Cζ–Cγ_2 Thr316	6.0 Å	4.0 Å	5.9 Å	3.9 Å
Phe403 Cζ–Cβ Asp315	3.7 Å	4.9 Å	6.1 Å	4.7 Å
Leu402 Cδ_2–Cγ_2 Thr316	4.4 Å	4.4 Å	6.2 Å	4.1 Å
Phe403 Cζ–C Ub-Gly76	–	4.3 Å	4.0 Å	4.2 Å
Phe403 Cζ/Cε_2–Cδ Ub-Lys63 (proximal)	–	–	–	4.1 Å/3.9 Å

residue turn segment, Leu402-Phe403, needs to move apart relative to Thr316 to make room for the diubiquitin substrate to position itself correctly in the active site. (These observations are also true in the structure of AMSH-LP bound to diubiquitin.) It seems likely that the β-turn segment is dynamic, fluctuating between open and closed forms; the substrate binds to the open form, perhaps by conformational selection. Superposition of all of our structures for the catalytic domain of free Sst2, ubiquitin-bound Sst2 (Sst2^{cat}–Ub and Sst2^{cat}E286A–Ub), and diubiquitin-bound Sst2 reveals that Leu402 and Phe403 are mobile (Figure 7a). The different mobility of side chains of Asp315, Leu402, and Phe403 shows that these three residues are involved in a conformational change between the free form and ubiquitin-bound form.

It is likely that the dynamics of the active-site flap may contribute to the recognition of specific Ub lysine linkages in addition to its role in catalysis. To probe whether the dynamics from this flap are associated with linkage specificity, we mutated Phe395 in AMSH to alanine (corresponding to the same residue as Phe403 in Sst2). The mutant exhibits significantly impaired catalytic activity;[20] however, like the wild-type enzyme, it was still unable to cleave Lys48-linked diubiquitin [we used up to 2 μM enzyme and 23 h reaction time, but failed to detect any product (Figure 7 of the Supporting Information)]. This observation does not rule out the possibility that dynamics of the flap could be a factor behind linkage specificity. More detailed studies using point mutants of the other residues from the flap and Thr316 and Asp315 are required to probe the contribution of the flap to linkage specificity. Of note, Sst2, unlike AMSH, appears to cleave Lys48-linked diubiquitin, albeit with an efficiency significantly

lower than that of the Lys63-linked chain. Under conditions in which formation of the product from K63-linked diubiquitin is essentially complete in 1 h, the enzyme takes nearly 24 h to produce an appreciable amount of product from Lys48-linked diubiquitin (see Figure 8 of the Supporting Information). The plant orthologue AMSH3 appears to be adept at cleaving both Lys63- and Lys48-linked chains.[69] It will be interesting to know the basis of relaxed specificity in going from AMSH to AMSH3 and if the dynamic nature of the flap is an underlying factor.

Structural Effect of the MIC-CAP Disease-Causing Thr to Ile Mutation. Recently, a whole-exome sequencing analysis led to the discovery of recessive mutations in the gene encoding AMSH that cause microcephaly capillary malformation (MIC-CAP) syndrome.[59] MIC-CAP syndrome, diagnosed at or shortly after birth, is characterized by severe microcephaly (a condition in which an infant's head is significantly smaller than the heads of other children of the same age and sex) with progressive cortical atrophy, intractable epilepsy, profound developmental delay, and excessive small capillary malformations on the skin.[38,70−72] The phenotype is attributed to the accumulation of ubiquitinated proteins, suggesting a loss of enzymatic function of AMSH, consistent with similar accumulation of polyubiquitinated species seen in knockout mice studies.[38,72] The study that discovered that mutations in AMSH could lead to MIC-CAP syndrome reported six missense mutations, two nonsense mutations, two translational frameshift mutations, and three intronic mutations.[59] Five of the six missense mutations occur within the MIT domain of AMSH, and the sixth, Thr313Ile, occurs within the JAMM domain. Because the crystal structure of AMSH bound to ubiquitin is not known, we took advantage of our structure to gain insights into possible effects the mutation may have on the structure of AMSH and its ubiquitin recognition.[59]

In Sst2, the corresponding residue is Thr319, which makes a hydrogen-bonding contact using its side-chain OH group with the backbone NH group of Leu73 of ubiquitin as seen in the structure of Sst2^{cat}–Ub (and other ubiquitin-bound structures reported here, as well). In the structure of Sst2^{cat}, this side chain is solvent-exposed. Mutation to Ile is unlikely to cause any serious perturbation to its overall three-dimensional structure. It thus appears that the mutation may weaken interactions with ubiquitin required for substrate recognition and/or catalysis. It is also possible that mutation to Ile may introduce additional steric clash with ubiquitin. To examine this, we generated an *in silico* model of the mutant based on the ubiquitin-bound structure of the wild-type enzyme and subjected it to refinement for generating a model with optimized contacts. The final model shows that isoleucine could be accommodated
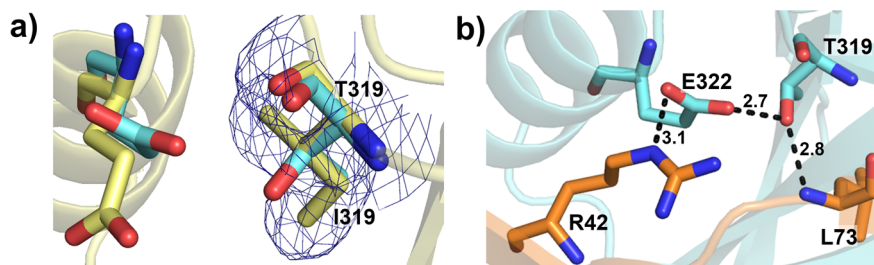

Figure 8. Structural consequences of the MIC-CAP mutation. (a) Superposition of Thr319 of Sst2^{cat} (aquamarine) and Ile319 of mutant Sst2^{cat}T319I (light yellow) showing the change in the orientation of Glu322. The electron density for Ile319 is rendered from the $2F_o − F_c$ map contoured at 1.2σ. (b) Hydrogen bonding interactions made by Thr319 observed in the Sst2^{cat}–Ub complex. Residues of Sst2 and Ub involved in interaction are colored aquamarine and orange, respectively. Hydrogen bonds are shown with black dashes.

in place of threonine without causing any serious steric clash with ubiquitin. Indeed, the X-ray structure of the Thr319Ile mutant of Sst2^{cat} in its free form reveals minimal changes in the protein structure adjacent to the Ile319, with the global structure of the mutant remaining largely unchanged relative to that of the wild-type enzyme. The most noticeable change in the Ile mutant was localized around the site of mutation: the side chain of Glu322, adjacent to Ile319, is oriented perpendicular to its original conformation in the free and ubiquitin-bound forms of Sst2^{cat} (Figure 8a). This is interesting because when ubiquitin is bound to Sst2^{cat}, Thr319 makes a hydrogen-bonding contact with Glu322 (distance of 2.6 Å between Oγ of Thr and Oδ of Glu), which is the only contact the latter residue makes with a protein atom. This contact appears to hold Glu322 in a position so that it could engage in hydrogen-bonding and electrostatic contacts with Arg42 of ubiquitin as seen in the crystal structure of Sst2^{cat}–Ub (Figure 8b). Thus, it is possible that substitution with Ile may lead to a loss of this interaction as well, explaining the substantial effect on the enzyme's catalytic activity (Table 5).

Table 5. Steady-State Kinetic Parameters of Sst2 and Its Substrate, Lys63-Linked Diubiquitin

sample	K_M (μM)	k_{cat} (s^{-1})	k_{cat}/K_M ($\times 10^{-3}$ μM^{-1} s^{-1})
Sst2	18.8 ± 8.4	1.5 ± 0.2	79.8
T319I	19.7 ± 4.0	0.043 ± 0.002	2.2
E286A	not determined	not determined	not determined

On the basis of the structural analysis presented above, we expected that loss of contacts with Leu73 and perhaps also with Arg42 of ubiquitin with the T319 mutant may destabilize the Michaelis complex relative to the wild-type enzyme. However, our kinetic analysis shows a substantial effect on k_{cat} with little change in K_M, consistent with results from a similar study with the Thr313Ile mutant of AMSH.[20] It appears that interactions involving the Thr residue are particularly important in aligning the scissile peptide bond in the proximity of the catalytic groups during formation of the transition state in the enzyme-catalyzed reaction.

A Reactive Cysteine Adjacent to the Active Site. A pair of cysteines (Cys288 and Cys317), with one of them adjacent to the catalytic site and solvent-exposed (Cys317), appears to be conserved within AMSH-like DUBs, as seen by comparison of the sequences of AMSH, AMSH-LP, and Sst2 (Figure 5 of the Supporting Information). The distance between the two thiol groups is 4.4 Å. Cys317 contributes to two interbackbone hydrogen bonds with Gly75 of ubiquitin. Interestingly, in two of our structures (Sst2$^{\Delta 220}$–K63-Ub$_2$ and the free form of Sst2^{cat} from the $P2_1$ space group), the $F_o - F_c$ map shows residual positive density that could be easily interpreted as an alternative rotameric conformation of Cys288, a conformation that brings the two cysteines within disulfide-forming distance, allowing us to model a disulfide bridge between the two cysteines (Figure 4f). It is possible that under oxidative conditions this pair will exist as a fully occupied disulfide bridge (DTT in our purification buffer may be responsible for reduction of the disulfide, giving us only a partial population of the oxidized form and none in other structures). A similar observation was also made in the case of AMSH, while a fully occupied disulfide bond was observed in AfJAMM, the first ever JAMM domain protein to be structurally characterized.[18,20] The reason behind the presence of the cysteine pair with the

potential to form this disulfide bond is not clear at the moment. One possibility may be the endosome-bound form requires the disulfide bond. Association with ESCRT-III through the MIT domain is required for deubiquitination of the cargo before formation of intraluminal vesicles in MVBs, an interaction that is especially tight ($K_D \sim 60$ nM).[73] It has been proposed that the VPS4 complex will catalyze the dissociation of AMSH from the ESCRT-III members at the end of MVB biogenesis so that the DUB and the ESCRT members can be reused for another around of endocytic sorting.[33,74] It is tempting to speculate that the disulfide bridge may render AMSH stable enough so that it can be dissociated from the ESCRT-III complex after the action of VPS4 but still remain folded.

■ DISCUSSION

As mentioned earlier, AMSH is thought to share distinct mechanistic similarities with the well-studied metalloprotease thermolysin.[23] On the basis of this assumed similarity with thermolysin, the mechanism of diubiquitin cleavage by AMSH and closely related enzymes (such as Sst2) is illustrated in Figure 9. Abstraction of a proton by the active-site glutamate (Glu286 in Sst2), the presumed general base, activates the zinc-bound water, converting it into a potent nucleophile. This nucleophilic water then attacks the carbonyl group of the scissile peptide bond, leading to a tetrahedral intermediate, which is stabilized by the interaction of the oxyanion with a nearby serine serving as the oxyanion-stabilizing residue [Ser351 in Sst2 (Figure 4e)]. The leaving group, the proximal ubiquitin, then departs, being aided by the transfer of a proton to the amine group by the same glutamic acid, now working as a proton donor. The departure of the leaving group is accompanied by the collapse of the tetrahedral intermediate forming the carboxylate group of the P (unprimed) fragment. At this stage, the carboxylate group of the P-product fragment, which corresponds to the distal ubiquitin in the diubiquitin substrate, is coordinated to the catalytic zinc (Figure 9). Finally, the P fragment dissociates, making room for the catalytic water to reestablish its coordinating position adjacent to the active-site zinc. The mechanism dictates that Glu286 be an essential residue for catalysis. In contrast, we observed that the Glu286Ala mutant of Sst2 still has some residual activity, much like the case of matrilysin,[65,75] suggesting that Glu286 in Sst2 may not be playing the role of the general base in the hydrolysis reaction. Instead, it may be required for stabilization of the transition state through hydrogen bonding with the carbonyl group of the scissile peptide bond and for donation of a proton to the leaving group. This is consistent with the observation that Glu286 is seen as the donor in the hydrogen bonding interaction with the carboxylate of Gly76 of ubiquitin (Figure 6 and Figure 6 of the Supporting Information) in our crystal structures. Because these crystals were grown from solutions with pH values ranging from 7 to 8, our data indicate that Glu286 may have a relatively high pK_a, at least 7, and would therefore remain protonated during catalysis. To be an effective general base, the glutamate must ionize readily below pH 7, as seen in the case of thermolysin.[76,77] Although the exact nature of the active-site Glu in Sst2 and related enzymes remains to be characterized, our structural studies point to the possibility that, in Sst2, the zinc-bound water may be ionized significantly to serve as the nucleophile directly, as was proposed for matrilysin.[65,75] Future studies aimed at delineating the pH dependence of activity should reveal more insight into the mechanism of Sst2 and related enzymes. Moreover,
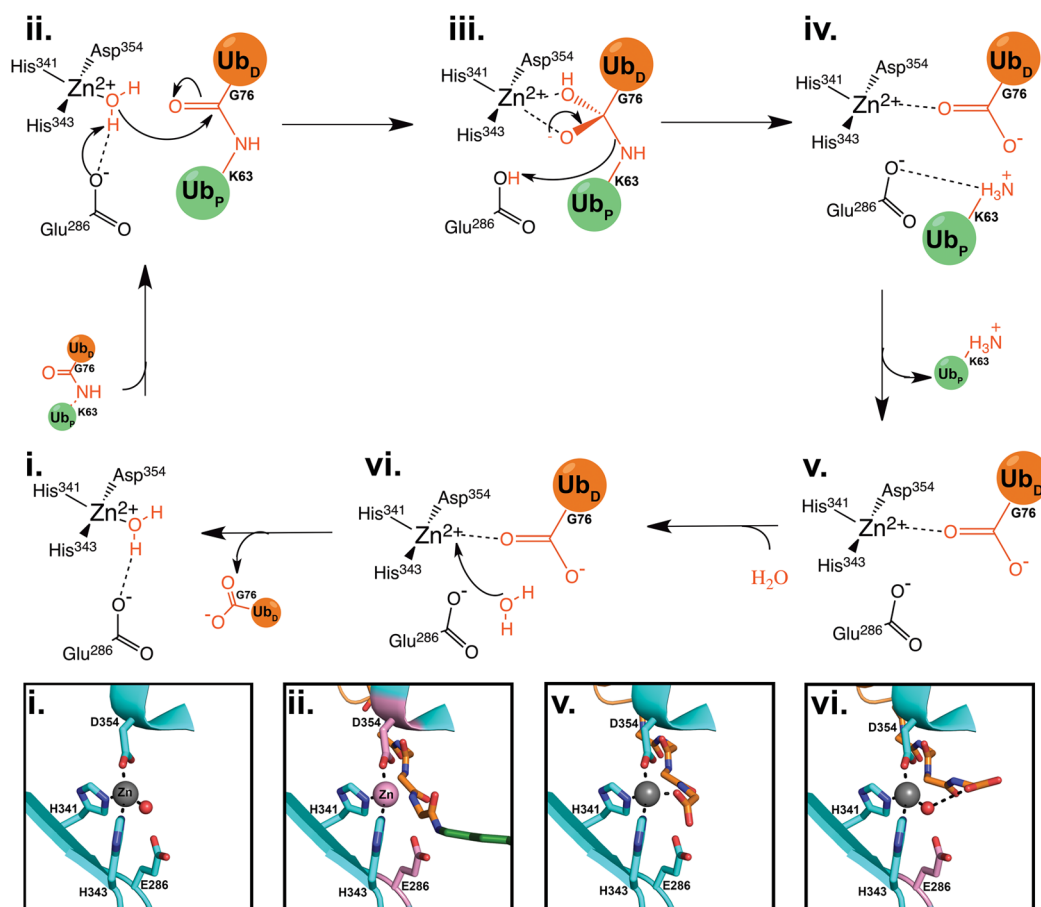
Figure 9. Proposed mechanism of hydrolysis by Sst2 and related enzymes, based on a thermolysin-like mechanism. UbP (green) denotes proximal ubiquitin, while UbD (orange) indicates distal ubiquitin. Steps of the mechanism that we have captured crystallographically are shown in boxes i., ii., v., and vi. In boxes ii. and vi., atoms that were modeled in because they were absent due to mutation are colored pink.
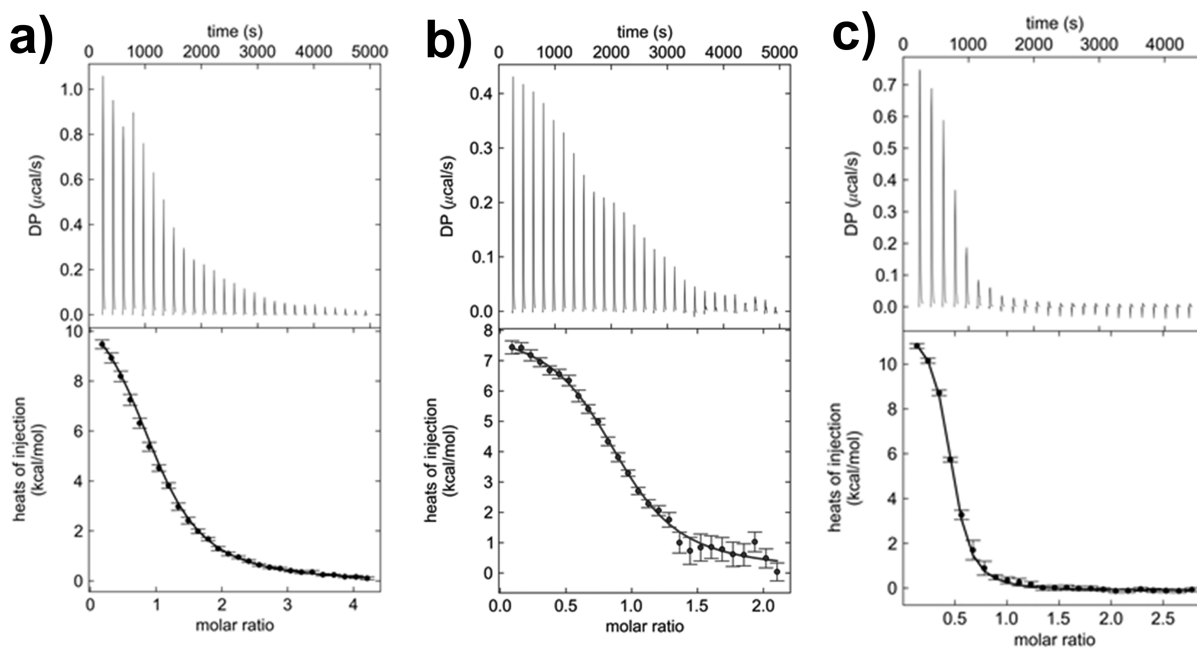

Figure 10. Isothermal titration calorimetry (ITC) thermograms of binding of ubiquitin to the catalytic domain of Sst2. (a) ITC thermogram of binding of ubiquitin to the catalytic domain of Sst2 revealing a K_D of 10.2 ± 0.6 μM. (b) ITC thermogram of binding of ubiquitin to the catalytic mutant of Sst2, E286A, revealing a K_D of 2.98 ± 0.56 μM. (c) ITC thermogram of binding of Lys63-linked diubiquitin to the catalytic mutant of Sst2, D354A, revealing a K_D of 1.1 ± 0.1.

mutation of Glu to Ala in thermolysin-like enzymes leads to loss of Zn, unlike the case for Sst2 and matrilysin. On the basis of these observations, we propose that Sst2 may behave more like matrilysin rather than like thermolysin. It remains to be seen whether AMSH and other related enzymes behave like Sst2.

In the context of diubiquitin hydrolysis, the fate of the P-product fragment after hydrolysis may become relevant as this fragment is engaged in a number of interactions with the enzyme. This is especially important because the binding to the substrate occurs predominantly through interactions of the distal ubiquitin (which corresponds to the P fragment of the substrate). The proximal ubiquitin does not seem to contribute significantly to substrate binding, although its interactions are important during the transition state of the reaction, as revealed by site-directed mutagenesis experiments with AMSH, which showed that mutation of residues that bind to the proximal ubiquitin affects k_{cat} but not K_M.[38] Consistent with this observation, isothermal titration calorimetry (ITC) studies reveal that like that of AMSH, Sst2's affinity for ubiquitin is similar to the K_M for diubiquitin hydrolysis (Figures 10 and 11).
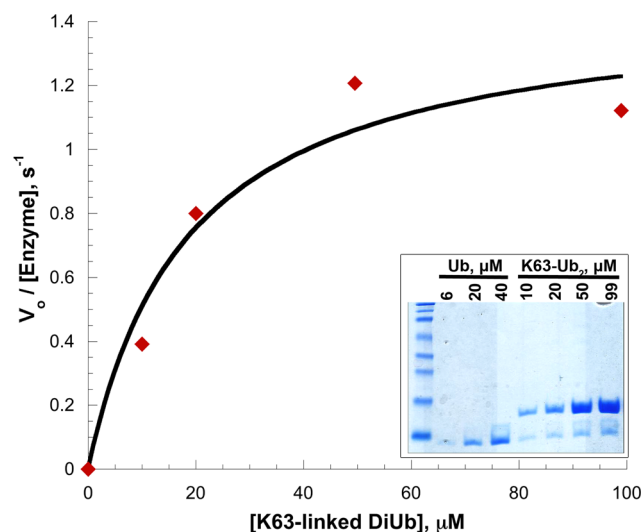

Figure 11. Representative plot of the initial velocity (divided by the total enzyme concentration) as a function of substrate concentration for wild-type Sst2. The inset shows a gel from kinetic reactions, showing ubiquitin standards and different concentrations of the substrate (K63-Ub$_2$) sampled. Each reaction mixture contained 25 nM Sst2^{cat}, and each reaction proceeded for 7.5 min at 20 °C before being quenched with 5× SDS−PAGE sample buffer. Bands corresponding to monoubiquitin were integrated using ImageJ.

Our structures provide insight into the nature of the interaction with the P-product fragment. All of the interactions with the distal ubiquitin of the substrate are still intact in the product-bound form. The major difference between the substrate-bound state and the product-bound state is with

respect to interactions of the Gln62-Lys63-Glu64 tripeptide segment with Phe4 of the proximal ubiquitin, interactions that would be relevant only to substrate binding but will be absent in the product. These interactions are replaced by interactions associated with metal-coordinating binding of the carboxylate group in the product-bound form. One of the carboxylate oxygens of ubiquitin's Gly76 occupies the void left by the nucleophilic water. The other oxygen is engaged in a hydrogen bonding interaction with Glu286 working as the hydrogen bond donor (the distance between the oxygen atoms is 2.7 Å). These interactions of the carboxylate on Gly76 of ubiquitin may contribute to the tight binding of the product, although, surprisingly, mutation of Glu286 to Ala did not result in any loss of ubiquitin affinity. In fact, the mutant actually appears to bind ubiquitin slightly stronger than the wild-type enzyme (Table 6). It is possible that the active-site structure in the mutant has changed, which might account for the anomalous behavior we are observing here. The role of Glu286 and ubiquitin's Gly76 interaction is therefore not clear at the moment. Nevertheless, our studies seem to provide a rationale for the observation that, for both AMSH and Sst2, the affinity for the product (K_D for ubiquitin) matches the K_M value observed with the diubiquitin substrate (Table 7). The

Table 7. Comparison of K_D and K_M between Sst2 and AMSH

enzyme	substrate or product	K_D (μM)	K_M (μM)
Sst2	ubiquitin	10.2 ± 0.6	−
Sst2^{cat}D354A	diubiquitin	1.1 ± 0.1	18.8
AMSH	ubiquitin	19 ± 3	−
AMSH	diubiquitin	19 ± 4	32 ± 5

structural data may provide a rationale for this observation if we assume that the carboxylate group of the product binding to zinc offsets the loss of interactions contributed by the proximal ubiquitin. This may imply that the free cytosolic form of AMSH may remain inhibited by binding to ubiquitin, as the concentration of free ubiquitin in cells is close to the K_D values we have measured.[78]

Proteases in general are tightly regulated, revealing their full catalytic potential only when desired. Several means of regulation of protease activity have been well characterized, examples of which include sequestration of proteases through compartmentalization, such as caspases,[79−83] proteasome,[84−86] and lysosomal proteases,[87−89] and conversion of precursor enzymes to active forms through zymogen activation,[90] such as digestive enzymes like trypsin and chymotrypsin, and reversible posttranslational modification. However, the mechanism underlying regulation of the catalytic activity of DUBs is relatively poorly understood.[91] Recent reports show that some cysteine DUBs can be regulated by reversible oxidation of their catalytic cysteine.[92,93] More generally, however, a substantial number of DUBs appear to be regulated via association with other proteins, including ubiquitin, serving as both a part of their substrates and their product.[94−97] Accordingly, a number of DUBs feature additional domains appended to or inserted into

Table 6. Thermodynamic Parameters Deduced from ITC Data

protein	titrant	K_D (μM)	ΔH (kcal/mol)	ΔS (cal mol^{-1} K^{-1})
Sst2	ubiquitin	10.2 ± 0.6	11.9 ± 0.4	62.9
Sst2^{cat}E286A	ubiquitin	3.0 ± 0.56	8.0 ± 0.7	52.2
Sst2^{cat}D354A	diubiquitin	1.1 ± 0.1	11.8 ± 0.3	66.9

their catalytic domain for associating with other proteins (activators), which in turn induce productive forms of the associated DUB.[14,15] Activation upon binding to other macromolecules can be allowed by realignment of active-site residues, if they were misaligned in the unbound state, or removal of steric occlusion by a conformational transition induced upon activator binding.[98,99] This is especially important for DUBs that exist in two distinct pools, in the free form when not bound to anything and in their active form as a population of protein-bound enzymes.

It appears from our studies that, for AMSH and related enzymes like Sst2, the close correspondence between the affinity for ubiquitin and the K_M value for the substrate may serve to regulate their catalytic activity. They could be inhibited when present in the free enzyme pool but manifest their full catalytic prowess upon assembly with other proteins, such as ESCRT-0 in the case of AMSH. Because the intracellular concentration of free ubiquitin is expected to be higher than that of the K63-linked polyubiquitin chain and is close to the dissociation constant for free ubiquitin (our studies),[78] one would expect the free enzyme would be inhibited. Assembly with other protein complexes may serve to activate these enzymes by providing additional factors that tip the balance toward better recognition of the substrate over free ubiquitin, such as the ubiquitin-binding UIM domain present in STAM, in whose case the UIM domain appears to provide additional strength to substrate binding by engaging with the proximal ubiquitin.[37]

ASSOCIATED CONTENT

Supporting Information

Supplemental Figures 1−8. This material is available free of charge via the Internet at http://pubs.acs.org.

Accession Codes

Coordinates and structure factors have been deposited in the PDB as entries 4JXE, 4MS7, 4MSJ (Sst2[cat]), 4K1R, 4MSQ (Sst2[cat]−Ub), 4MSM (Sst2[cat]E286A−Ub), 4NQL (Sst2[Δ220]−K63-Ub$_2$), 4PQT (Sst2[cat]D354A−Ub), and 4MSD (Sst2[cat]T319I).

AUTHOR INFORMATION

Corresponding Author

*Brown Laboratory of Chemistry, 560 Oval Dr., West Lafayette, IN 47907. E-mail: cdas@purdue.edu. Phone: (765) 494-5478. Fax: (765) 494-0239.

Author Contributions

R.K.S. and J.A.R. contributed equally to this work.

ACKNOWLEDGMENTS

ABBREVIATIONS

DUB, deubiquitinating enzyme; JAMMs, JAB1/MPN/MOV34 metalloenzymes; AMSH, associated molecule with the SH3 domain of STAM; ESCRT, endosomal sorting complexes required for transport; UIM, ubiquitin-interacting motif; SH3, SRC homology; Sst2, AMSH-like protease Sst2; GST, glutathione *S*-transferase; PDB, Protein Data Bank; IPTG, isopropyl β-D-thiogalactoside; SEC, size exclusion chromatography; K63-Ub$_2$, Lys63-linked diubiquitin; PEG, poly(ethylene glycol).

REFERENCES

(1) Hershko, A., and Ciechanover, A. (1998) The ubiquitin system. *Annu. Rev. Biochem. 67*, 425−479.

(2) Glickman, M. H., and Ciechanover, A. (2002) The ubiquitin-proteasome proteolytic pathway: Destruction for the sake of construction. *Physiol. Rev. 82*, 373−428.

(3) Varshavsky, A. (1997) The ubiquitin system. *Trends Biochem. Sci. 22*, 383−387.

(4) Mattiroll, F., and Sixma, T. (2014) Lysine-targeting specificity in ubiquitin and ubiquitin-like modification pathways. *Nat. Struct. Mol. Biol. 21*, 308−316.

(5) Komander, D., and Rape, M. (2012) The ubiquitin code. *Annu. Rev. Biochem. 81*, 203−229.

(6) Schulman, B., and Harper, J. (2009) Ubiquitin-like protein activation by E1 enzymes: The apex for downstream signaling pathways. *Nat. Rev. Mol. Cell Biol. 10*, 319−331.

(7) Pickart, C., and Eddins, M. (2004) Ubiquitin: Structures, functions, mechanisms. *Biochim. Biophys. Acta 1695*, 55−72.

(8) Haglund, K., and Dikic, I. (2005) Ubiquitylation and cell signaling. *EMBO J. 24*, 3353−3359.

(9) Ikeda, F., and Dikic, I. (2008) Atypical ubiquitin chains: New molecular signals. 'Protein Modifications: Beyond the Usual Suspects' review series. *EMBO Rep. 9*, 536−542.

(10) Pickart, C. M. (2000) Ubiquitin in chains. *Trends Biochem. Sci. 25*, 544−548.

(11) Reyes-Turcu, F. E., Ventii, K. H., and Wilkinson, K. D. (2009) Regulation and cellular roles of ubiquitin-specific deubiquitinating enzymes. *Annu. Rev. Biochem. 78*, 363−397.

(12) D'Andrea, A., and Pellman, D. (1998) Deubiquitinating enzymes: A new class of biological regulators. *Crit. Rev. Biochem. Mol. Biol. 33*, 337−352.

(13) Love, K., Catic, A., Schlieker, C., and Ploegh, H. (2007) Mechanisms, biology and inhibitors of deubiquitinating enzymes. *Nat. Chem. Biol. 3*, 697−705.

(14) Komander, D., Clague, M. J., and Urbe, S. (2009) Breaking the chains: Structure and function of the deubiquitinases. *Nat. Rev. Mol. Cell Biol. 10*, 550−563.

(15) Nijman, S., Luna-Vargas, M., Velds, A., Brummelkamp, T., Dirac, A., Sixma, T., and Bernards, R. (2005) A genomic and functional inventory of deubiquitinating enzymes. *Cell 123*, 773−786.

(16) Komander, D. (2010) Mechanism, specificity and structure of the deubiquitinases. *Subcell. Biochem. 54*, 69−87.

(17) Wilkinson, K. D. (2009) DUBs at a glance. *J. Cell Sci. 122*, 2325−2329.

(18) Ambroggio, X. I., Rees, D. C., and Deshaies, R. J. (2004) JAMM: A metalloprotease-like zinc site in the proteasome and signalosome. *PLoS Biol. 2*, 113−119.

(19) Amerik, A. Y., and Hochstrasser, M. (2004) Mechanism and function of deubiquitinating enzymes. *Biochim. Biophys. Acta 1695*, 189−207.

(20) Davies, C. W., Paul, L. N., Kim, M. I., and Das, C. (2011) Structural and Thermodynamic Comparison of the Catalytic Domain

of AMSH and AMSH-LP: Nearly Identical Fold but Different Stability. *J. Mol. Biol. 413*, 416−429.

(21) Sobhian, B., Shao, G. Z., Lilli, D. R., Culhane, A. C., Moreau, L. A., Xia, B., Livingston, D. M., and Greenberg, R. A. (2007) RAP80 targets BRCA1 to specific ubiquitin structures at DNA damage sites. *Science 316*, 1198−1202.

(22) Kikuchi, K., Ishii, N., Asao, H., and Sugamura, K. (2003) Identification of AMSH-LP containing a Jab1/MPN domain metalloenzyme motif. *Biochem. Biophys. Res. Commun. 306*, 637−643.

(23) Sato, Y., Yoshikawa, A., Yamagata, A., Mimura, H., Yamashita, M., Ookata, K., Nureki, O., Iwai, K., Komada, M., and Fukai, S. (2008) Structural basis for specific cleavage of Lys 63-linked polyubiquitin chains. *Nature 455*, 358−362.

(24) Verma, R., Aravind, L., Oania, R., McDonald, W. H., Yates, J. R., III, Koonin, E. V., and Deshaies, R. J. (2002) Role of Rpn11 metalloprotease in deubiquitination and degradation by the 26S proteasome. *Science 298*, 611−615.

(25) Yao, T., and Cohen, R. E. (2002) A cryptic protease couples deubiquitination and degradation by the proteasome. *Nature 419*, 403−407.

(26) Echalier, A., Pan, Y., Birol, M., Tavernier, N., Pintard, L., Hoh, F., Ebel, C., Galophe, N., Claret, F., and Dumas, C. (2013) Insights into the regulation of the human COP9 signalosome catalytic subunit, CSN5/Jab1. *Proc. Natl. Acad. Sci. U.S.A. 110*, 1273−1278.

(27) Guterman, A., and Glickman, M. (2004) Deubiquitinating enzymes are IN/(trinsic to proteasome function). *Curr. Protein Pept. Sci. 5*, 201−211.

(28) Saksena, S., Sun, J., Chu, T., and Emr, S. D. (2007) ESCRTing proteins in the endocytic pathway. *Trends Biochem. Sci. 32*, 561−573.

(29) Wollert, T., Wunder, C., Lippincott-Schwartz, J., and Hurley, J. H. (2009) Membrane scission by the ESCRT-III complex. *Nature 458*, 172−177.

(30) McCullough, J., Clague, M. J., and Urbe, S. (2004) AMSH is an endosome-associated ubiquitin isopeptidase. *J. Cell Biol. 166*, 487−492.

(31) Raiborg, C., and Stenmark, H. (2009) The ESCRT machinery in endosomal sorting of ubiquitylated membrane proteins. *Nature 458*, 445−452.

(32) Henne, W. M., Buchkovich, N. J., and Emr, S. D. (2011) The ESCRT Pathway. *Dev. Cell 21*, 77−91.

(33) Wollert, T., and Hurley, J. H. (2010) Molecular mechanism of multivesicular body biogenesis by ESCRT complexes. *Nature 464*, 864−869.

(34) Mizuno, E., Kobayashi, K., Yamamoto, A., Kitamura, N., and Komada, M. (2006) A deubiquitinating enzyme UBPY regulates the level of protein ubiquitination on endosomes. *Traffic 7*, 1017−1031.

(35) Row, P. E., Prior, I. A., McCullough, J., Clague, M. J., and Urbe, S. (2006) The ubiquitin isopeptidase UBPY regulates endosomal ubiquitin dynamics and is essential for receptor down-regulation. *J. Biol. Chem. 281*, 12618−12624.

(36) Avvakumov, G., Walker, J., Xue, S., Finerty, P., Jr., Mackenzie, F., Newman, E., and Dhe-Paganon, S. (2006) Amino-terminal dimerization, NRDP1-rhodanese interaction, and inhibited catalytic domain conformation of the ubiquitin-specific protease 8 (USP8). *J. Biol. Chem. 281*, 38061−38070.

(37) Clague, M. J., and Urbé, S. (2006) Endocytosis: The DUB version. *Trends Cell Biol. 16*, 551−559.

(38) Davies, C. W., Paul, L. N., and Das, C. (2013) Mechanism of Recruitment and Activation of the Endosome-Associated Deubiquitinase AMSH. *Biochemistry 52*, 7818−7829.

(39) Trang, V. H., Valkevich, E. M., Minami, S., Chen, Y. C., Ge, Y., and Strieter, E. R. (2012) Nonenzymatic polymerization of ubiquitin: Single-step synthesis and isolation of discrete ubiquitin oligomers. *Angew. Chem., Int. Ed. 51*, 13085−13088.

(40) Otwinowski, Z., and Minor, W. (1997) Processing of X-ray diffraction data collected in oscillation mode. *Methods Enzymol. 276*, 307−326.

(41) Vagin, A. A., and Teplyakov, A. (1997) MOLREP: An Automated Program for Molecular Replacement. *J. Appl. Crystallogr. 30*, 1022−1025.

(42) Collaborative Computational Project, Number 4 (1994) The CCP4 suite: Programs for protein crystallography. *Acta Crystallogr. D50*, 760−763.

(43) Arnold, K., Bordoli, L., Kopp, J., and Schwede, T. (2006) The SWISS-MODEL workspace: A web based environment for protein structure homology modeling. *Bioinformatics 22*, 195−201.

(44) Murshudov, G. N., Vagin, A. A., and Dodson, E. J. (1997) Refinement of Macromolecular Structures by the Maximum-Likelihood Method. *Acta Crystallogr. D53*, 240−255.

(45) Emsley, P., Lohkamp, B., Scott, W. G., and Cowtan, K. (2010) Features and development of Coot. *Acta Crystallogr. D66*, 486−501.

(46) Adams, P. D., Grosse Kunstleve, R. W., Hung, L. W., Ioerger, T. R., McCoy, A. J., Moriarty, N. W., Read, R. J., Sacchettini, J. C., Sauter, N. K., and Terwilliger, T. C. (2002) PHENIX: Building new software for automated crystallographic structure determination. *Acta Crystallogr. D58*, 1948−1954.

(47) Adams, P. D., Afonine, P. V., Bunkoczi, G., Chen, V. B., Davis, I. W., Echols, N., Headd, J. J., Hung, L.-W., Kapral, G. J., and Grosse-Kunstleve, R. W. (2010) PHENIX: A comprehensive Python-based system for macromolecular structure solution. *Acta Crystallogr. D66*, 213−221.

(48) Painter, J., and Merritt, E. A. (2006) Optimal description of a protein structure in terms of multiple groups undergoing TLS motion. *Acta Crystallogr. D62*, 439−450.

(49) Painter, J., and Merritt, E. A. (2006) TLSMD web server for the generation of multi-group TLS models. *J. Appl. Crystallogr. 39*, 109−111.

(50) Terwilliger, T., Adams, P., Read, R., McCoy, A., Moriarty, N., Grosse-Kunstleve, R., Afonine, P., Zwart, P., and Hung, L. (2009) Descision-making in structure solution using Bayesian estimates of map quality: The PHENIX AutoSol wizard. *Acta Crystallogr. D65*, 582−601.

(51) McCoy, A. J., Grosse-Kunstleve, R. W., Adams, P. D., Winn, M. D., Storoni, L. C., and Read, R. J. (2007) Phaser crystallographic software. *J. Appl. Crystallogr. 40*, 658−674.

(52) Terwilliger, T. (2002) Automated structure solution, density modification and model building. *Acta Crystallogr. D58*, 1937−1940.

(53) *The PyMOL Molecular Graphics System*, version 1.5.0.4 (2010) Schrödinger, LLC, Portland, OR.

(54) Schneider, C. A., Rasband, W. S., and Eliceiri, K. W. (2012) NIH Image to ImageJ: 25 years of image analysis. *Nat. Methods 9*, 671−675.

(55) Keller, S., Vargas, C., Zhao, H., Piszczek, G., Brautigam, C. A., and Schuck, P. (2012) High-precision isothermal titration calorimetry with automated peak-shape analysis. *Anal. Chem. 84*, 5066−5073.

(56) Houtman, J. C., Brown, P. H., Bowden, B., Yamaguchi, H., Appella, E., Samelson, L. E., and Schuck, P. (2007) Studying multisite binary and ternary protein interactions by global analysis of isothermal titration calorimetry data in SEDPHAT: Application to adaptor protein complexes in cell signaling. *Protein Sci. 16*, 30−42.

(57) Lipscomb, W. N., and Sträter, N. (1996) Recent Advances in Zinc Enzymology. *Chem. Rev. 96*, 2375−2433.

(58) Vazeux, G., Wang, J., Corvol, P., and Llorens-Cortès, C. (1996) Identification of Glutamate Residues Essential for Catalytic Activity and Zinc Coordination in Aminopeptidase A. *J. Biol. Chem. 271*, 9069−9074.

(59) McDonell, L. M., Mirzaa, G. M., Alcantara, D., Schwartzentruber, J., Carter, M. T., Lee, L. J., Clericuzio, C. L., Graham, J. M., Jr., Morris-Rosendahl, D. J., Polster, T., Acsadi, G., Townshend, S., Williams, S., Halbert, A., Isidor, B., David, A., Smyser, C. D., Paciorkowski, A. R., Willing, M., Woulfe, J., Das, S., Beaulieu, C. L., Marcadier, J., Geraghty, M. T., Frey, B. J., Majewski, J., Bulman, D. E., Dobyns, W. B., O'Driscoll, M., and Boycott, K. M. (2013) Mutations in STAMBP, encoding a deubiquitinating enzyme, cause microcephaly-capillary malformation syndrome. *Nat. Genet. 45*, 556−562.

(60) Pena, V., Liu, S., Bujnicki, J. M., Luhrmann, R., and Wahl, M. C. (2007) Structure of a multipartite protein-protein interaction domain

in splicing factor prp8 and its link to retinitis pigmentosa. *Mol. Cell 25*, 615−624.

(61) Tran, H. J., Allen, M. D., Lowe, J., and Bycroft, M. (2003) Structure of the Jab1/MPN domain and its implications for proteasome function. *Biochemistry 42*, 11460−11465.

(62) Zhang, L., Shen, J., Guarnieri, M. T., Heroux, A., Yang, K., and Zhao, R. (2007) Crystal structure of the C-terminal domain of splicing factor Prp8 carrying retinitis pigmentosa mutants. *Protein Sci. 16*, 1024−1031.

(63) Birol, M., and Echalier, A. (2014) Structure and Function of MPN (Mpr1/Pad1 N-Terminal) Domain-Containing Proteins. *Curr. Protein Pept. Sci.*, in press.

(64) Krissinel, E., and Henrick, K. (2007) Inference of macromolecular assemblies from crystalline state. *J. Mol. Biol. 372*, 774−797.

(65) Johnson, L. L., Pavlovsky, A. G., Johnson, A. R., Janowicz, J. A., Man, C.-F., Ortwine, D. F., Purchase, C. F., II, White, A. D., and Hupe, D. J. (2000) A Rationalization of the Acidic pH Dependence for Stromelysin-1 (Matrix Metalloproteinase-3) Catalysis and Inhibition. *J. Biol. Chem. 275*, 11026−11033.

(66) Beal, R., Deveraux, Q., Xia, G., Rechsteiner, M., and Pickart, C. (1996) Surface hydrophobic residues of multiubiquitin chains essential for proteolytic targeting. *Proc. Natl. Acad. Sci. U.S.A. 93*, 861−866.

(67) Shih, S. C., Sloper-Mould, K. E., and Hicke, L. (2000) Monoubiquitin carries a novel internalization signal that is appended to activated receptors. *EMBO J. 19*, 187−198.

(68) Hurley, J. H., Lee, S., and Prag, G. (2006) Ubiquitin-binding domains. *Biochem. J. 399*, 361−372.

(69) Katsiarimpa, A., Muñoz, A., Kalinowska, K., Uemura, T., Rojo, E., and Isono, E. (2014) The ESCRT-III-Interacting Deubiquitinating Enzyme AMSH3 is Essential for Degradation of Ubiquitinated Membrane Proteins in *Arabidopsis thaliana*. *Plant Cell Physiol. 55*, 727−736.

(70) Carter, M. T., and Boycott, K. M. (2011) Microcephaly-capillary malformation syndrome: A story of rapid emergence of a new recognizable entity. *Am. J. Med. Genet., Part A 155A*, 2078−2079.

(71) Mirzaa, G. M., Paciorkowski, A. R., Smyser, C. D., Willing, M. C., Lind, A. C., and Dobyns, W. B. (2011) The microcephaly-capillary malformation syndrome. *Am. J. Med. Genet., Part A 155A*, 2080−2087.

(72) Suzuki, S., Tamai, K., Watanabe, M., Kyuuma, M., Ono, M., Sugamura, K., and Tanaka, N. (2011) AMSH is required to degrade ubiquitinated proteins in the central nervous system. *Biochem. Biophys. Res. Commun. 408*, 582−588.

(73) Solomons, J., Sabin, C., Poudevigne, E., Usami, Y., Hulsik, D. L., Macheboeuf, P., Hartlieb, B., Göttlinger, H., and Weissenhorn, W. (2011) Structural Basis for ESCRT-III CHMP3 Recruitment of AMSH. *Structure 19*, 1149−1159.

(74) Teis, D., Saksena, S., and Emr, S. D. (2008) Ordered Assembly of the ESCRT-III Complex on Endosomes Is Required to Sequester Cargo during MVB Formation. *Dev. Cell 15*, 578−589.

(75) Cha, J., and Auld, D. S. (1997) Site-directed mutagenesis of the active site glutamate in human matrilysin: Investigation of its role in catalysis. *Biochemistry 36*, 16019−16024.

(76) Matthews, B. (1988) Structural basis of the action of thermolysin and related zinc peptidases. *Acc. Chem. Res. 21*, 333−340.

(77) Grams, F., Reinemer, P., Powers, J., Kleine, T., Pieper, M., Tschesche, H., Huber, R., and Bode, W. (1995) X-ray structures of human neutrophil collagenase complexed with peptide hydroxamate and peptide thiol inhibitors: Implications for substrate and rational drug design. *Eur. J. Biochem. 228*, 830−841.

(78) Kaiser, S. E., Riley, B. E., Shaler, T. A., Trevino, R. S., Becker, C. H., Schulman, H., and Kopito, R. R. (2011) Protein standard absolute quantification (PSAQ) method for the measurement of cellular ubiquitin pools. *Nat. Methods 8*, 691−696.

(79) Martin, D., Siegel, R., Zheng, L., and Lenardo, M. (1998) Membrane oligomerization and cleavage activates the caspase-8 (FLICE/MACHalpha1) death signal. *J. Biol. Chem. 273*, 4345−4349.

(80) Schug, Z., Gonzalvez, F., Houtkooper, R., Vaz, F., and Gottlieb, E. (2011) BID is cleaved by caspase-8 within a native complex on the mitochondrial membrane. *Cell Death Differ. 18*, 538−548.

(81) Kantari, C., and Walczak, H. (2011) Caspase-8 and bid: Caught in the act between death receptors and mitochondria. *Biochim. Biophys. Acta 1813*, 558−563.

(82) Jin, Z., Li, Y., Pitt, R., Lawrence, D., Pham, V., Lill, J., and Ashkenazi, A. (2009) Cullin3-based polyubiquitination and p62-dependent aggregation of caspase-8 mediate extrinsic apoptosis signaling. *Cell 137*, 721−735.

(83) Beaudouin, J., Liesche, C., Aschenbrenner, S., Hörner, M., and Eils, R. (2013) Caspase-8 cleaves its substrates from the plasma membrane upon CD95-induced apoptosis. *Cell Death Differ. 20*, 599−610.

(84) Groll, M., and Clausen, T. (2003) Molecular shredders: How proteasomes fulfill their role. *Curr. Opin. Struct. Biol. 13*, 665−673.

(85) Pickart, C., and Cohen, R. (2004) Proteasomes and their kin: Proteases in the machine age. *Nat. Rev. Mol. Cell Biol. 5*, 177−187.

(86) Baumeister, W., Walz, J., Zühl, F., and Seemüller, E. (1998) The proteasome: Paradigm of a self-compartmentalizing protease. *Cell 92*, 367−380.

(87) Dragonetti, A., Baldassarre, M., Castino, R., Démoz, M., Luini, A., Buccione, R., and Isidoro, C. (2000) The lysosomal protease cathepsin D is efficiently sorted to and secreted from the regulated secretory compartments in the rat basophilic/mast cell line RBL. *J. Cell Sci. 113*, 3289−3298.

(88) Brumell, J., Volchuck, A., Sengelov, H., Borregaard, N., Cieutat, A., Bainton, D., Grinstein, S., and Klip, A. (1995) Subcellular distribution of docking/fusion proteins in neutrophils, secretory cells with multiple exocytic compartments. *J. Immunol. 155*, 5750−5759.

(89) Stinchcombe, J., and Griffiths, G. (1999) Regulated secretion of hemopoietic cells. *J. Cell Biol. 147*, 1−5.

(90) Stroud, R., Kossiakoff, A., and Chambers, J. (1977) Mechanisms of zymogen activation. *Annu. Rev. Biophys. Bioeng. 6*, 177−193.

(91) Huang, O., and Cochran, A. (2013) Regulation of deubiquitinase proteolytic activity. *Curr. Opin. Struct. Biol. 23*, 806−811.

(92) Cotto-Rios, X. M., Bekes, M., Chapman, J., Ueberheide, B., and Huang, T. T. (2012) Deubiquitinases as a Signaling Target of Oxidative Stress. *Cell Rep. 2*, 1475−1484.

(93) Kulathu, Y., Garcia, F., Mevissen, T., Busch, M., Arnaudo, N., Carroll, K., Barford, D., and Komander, D. (2013) Regulation of A20 and other OTU deubiquitinases by reversible oxidation. *Nat. Commun. 4*, 1569.

(94) Boudreaux, D., Maiti, T., Davies, C., and Das, C. (2010) Ubiquitin vinyl methyl ester binding orients the misaligned active site of the ubiquitin hydrolase UCHL1 into productive conformation. *Proc. Natl. Acad. Sci. U.S.A. 107*, 9117−9122.

(95) Hu, M., Li, P., Li, M., Li, W., Yao, T., Wu, J., Gu, W., Cohen, R., and Shi, Y. (2002) Crystal structure of a UBP-family deubiquitinating enzyme in isolation and in complex with ubiquitin aldehyde. *Cell 111*, 1041−1054.

(96) Keusekotten, K., Elliott, P., Glockner, L., Fill, B., Damgaard, R., Kulathu, Y., Wauer, T., Hospenthal, M., Gyrd-Hansen, M., Krappmann, D., Hofmann, K., and Komander, D. (2013) OTULIN antagonizes LUBAC signaling by specifically hydrolyzing Met1-linked polyubiquitin. *Cell 153*, 1312−1326.

(97) Faesen, A., Dirac, A., Shanmugham, A., Ovaa, H., Perrakis, A., and Sixma, T. (2011) Mechanism of USP7/HAUSP activation by its C-terminal ubiquitin-like domain and allosteric regulation by GMP-synthetase. *Mol. Cell 44*, 147−159.

(98) Samara, N., Datta, A., Berndsen, C., Zhang, X., Yao, T., Cohen, R., and Wolberger, C. (2010) Structural insights into the assembly and function of the SAGA deubiquitinating module. *Science 328*, 1025−1029.

(99) Yao, T., Song, L., Xu, W., DeMartino, G., Florens, L., Swanson, S., Washburn, M., Conaway, R., Conaway, J., and Cohen, R. (2006) Proteasome recruitment and activation of the Uch37 deubiquitinating enzyme by Adrm1. *Nat. Cell Biol. 8*, 994−1002.